People`s Democratic Republic of Algeria

Ministry of Higher Education and Scientific Research

University of Echahid Hamma Lakhdar - El Oued

Faculty of Technology

Department of Mechanical Engineering

Dissertation

ACADEMIC MASTER

Domain: **Science and Technology**

Division: **Mechanical Engineering**

Specialty: **Renewable energies**

Presented by:

Achouak Chihane

Entitled:

Optimizing Solar Thermal Output: A Comparative Study of Flat-Plate

Dissertation Submitted in Partial Fulfillment of the Requirements for the Master on Renewable energies Degree in Master ER

Publicly defended in: 19/06 /2026

Board of Examiners:

Dr. DEGHOUM Khalil	**Chairman**
Dr. HORR Sabrina	**Supervisor**
Dr. KHECHEKHOUCHE Abderrahmane	**Co supervisor**
Prof. AOUN Yassine	**Examiner**

Academic Year: 2025/2026

Acknowledgements

Praise be to Allah, Glory be to Him, who has bestowed upon me both outward and inward blessings and honored me with the blessing of Islam and monotheism. All praise is due to Him for His generosity, assistance, kindness, strength, and power, through which this humble work has been accomplished. I extend my sincere gratitude and appreciation to **Dr. Horr Sabrina** and **Dr. Khechekhouche Abderrahmane** for their valuable guidance and continuous support throughout the preparation of this Master’s thesis, as they were truly exemplary supervisors and mentors.
I also express my deepest appreciation and gratitude to the Head of the Department of Mechanical Engineering, **Pr. Meneceur Ridha**, for his administrative and scientific support during the completion of this work. Furthermore, I would like to extend my sincere thanks to the Head of the Laboratory of Modern Technologies and Local Development **Dr. Miloudi Abdelmonem** as well as to all members of the laboratory. Special thanks are also extended to the Director of the Research Unit Development of Renewable Energies **Pr. Mohammed El Tayeb Oucif Khaled** in addition to all members of the unit in appreciation of their support and assistance.

My sincere appreciation is extended to **Pr. Aoun Yassine** for serving as an examiner of this Master's thesis and to **Dr. Deghoum Khalil** for chairing the examination committee. I am truly grateful for their valuable time, thoughtful evaluation, and creative recommendations, which have greatly contributed to the enhancement of this dissertation.

Finally, I would like to thank everyone who offered me help advice encouragement or support even through sincere prayers from afar. I also apologies to anyone who contributed to the completion of this thesis whose name may have been unintentionally omitted from this page.

Dedication

To my dear parents – may God preserve them for me – and to everyone who has chosen the path of knowledge realizing that it is a weapon against evil and a light for insight and who has fought against ignorance despite all the hardships and obstacles and to all those who have offered me support and encouragement throughout my academic journey and to my brothers and sisters and everyone in my extended family I dedicate this
work

Abstract

This thesis investigates the enhancement of flat-plate solar collector performance using recycled aluminum shavings integrated into the absorber surface. Three collector prototypes were experimentally tested under natural and forced convection conditions: a reference collector, a collector with 20 g of aluminum shavings, and a collector with 40 g of aluminum shavings. The results showed that the addition of aluminum shavings improved heat transfer and thermal efficiency. Prototype 3 (40 g) achieved the best thermal performance and the highest efficiency under both operating modes. The study demonstrates that recycled aluminum shavings provide a simple, economical, and effective solution for improving solar collector performance. Keywords: Solar energy, Flat-plate solar collector, Thermal efficiency, Aluminum shavings, Heat transfer.

Résumé

Ce mémoire étudie l'amélioration des performances thermiques des capteurs solaires plans grâce à l'intégration de copeaux d'aluminium recyclés sur la surface de l'absorbeur. Trois prototypes ont été testés expérimentalement sous convection naturelle et forcée : un capteur de référence, un capteur contenant 20 g de copeaux d'aluminium et un autre contenant 40 g. Les résultats ont montré que l'ajout de copeaux d'aluminium améliore le transfert de chaleur et le rendement thermique. Le prototype 3 (40 g) a obtenu les meilleures performances thermiques et le rendement le plus élevé. Cette étude confirme que les copeaux d'aluminium recyclés constituent une solution simple, économique et efficace pour améliorer les performances des capteurs solaires. Mots-clés : Énergie solaire, Capteur solaire plan, Rendement thermique, Copeaux d'aluminium, Transfert de chaleur.

الملخص

تهدف هذه المذكرة إلى دراسة تحسين الأداء الحراري للمجمعات الشمسية المسطحة باستعمال برادة الألمنيوم المعاد تدويرها على سطح الماص. تم اختبار ثلاثة نماذج تجريبياً تحت الحمل الطبيعي والحمل القسري: نموذج مرجعي، ونموذج يحتوي على 20 غ من برادة الألمنيوم، ونموذج يحتوي على 40 غ. أظهرت النتائج أن إضافة برادة الألمنيوم ساهمت في تحسين انتقال الحرارة ورفع الكفاءة الحرارية. كما حقق النموذج الثالث (40 غ) أفضل أداء حراري وأعلى كفاءة مقارنة ببقية النماذج. تؤكد الدراسة أن استخدام برادة الألمنيوم المعاد تدويرها يمثل حلاً بسيطاً واقتصادياً وفعالاً لتحسين أداء المجمعات الشمسية .الكلمات المفتاحية: الطاقة الشمسية، المجمع الشمسي المسطح، الكفاءة الحرارية، برادة الألمنيوم، انتقال الحراري

Summray

List of Figure

List of Table

Nomenclatures

Symbol	Definition	Unit
A_c	Clear aperture area of a single solar collector	M^2
C_p	Specific heat capacity of the working fluid	J/kg.K
G	Total global solar radiation incident on the collector surface	W/m^2
h	Convective heat transfer coefficient inside the riser tubes	W/m^2. K
k	Thermal conductivity of the coating material (e.g., Al powder)	W/m. K
$\dot{m}$	Mass flow rate of the working fluid	kg/s}or m^3/h
Q_{solar}	Total solar radiation energy incident upon the collector aperture	W
Q_{useful}	Useful heat power gained by the working fluid	W
T_{abs}	Absorber plate temperature	°C
$T_{abs.max}$	Maximum peak absorber plate temperature	°C
T_{amb}	Ambient temperature	°C
$T_{chamber}$	Internal cavity / chamber room temperature	°C
$T_{chamber.max}$	Maximum peak internal chamber room temperature	°C
T_{Gex}	External glass cover surface temperature	°C
$T_{Gex.max}$	Maximum peak external glass temperature	°C
T_{Gint}	Internal glass cover surface temperature	°C
$T_{Gint.max}$	Maximum peak internal glass temperature	°C
T_{in}	Inlet fluid temperature entering the collector loop	°C
T_{out}	Outlet fluid temperature discharging from the collector	°C
$T_{out.max}$	Maximum peak outlet fluid temperature	°C
T_{room}	Air cavity or room temperature inside the casing	°C
ΔT	Temperature difference	°C or K

Abbreviations

Abbreviation	Full Description
Al	Aluminum
CO_2	Carbon Dioxide
$Flow_{.Out}$	Fluid Outlet Volume/Mass Flow Rate
FPC	Flat-Plate Solar Collector
$G_{1ex}t$ / G_{2ext} / G_{3ext}	External Glass Cover Temperatures for Collectors 1, 2, and 3
G_{1int} / $G_{2in}t$ / G_{3int}	Internal Glass Cover Temperatures for Collectors 1, 2, and 3
Reference	Untreated baseline collector layout (Collector 1)
T_{Abs1} / T_{Abs2} / T_{Abs3}	Absorber Plate Elements for Collectors 1, 2, and 3
T_{Chamb1} / T_{Chamb2} / T_{Chamb3}	Inner Chamber/Room Air Temperature for Collectors 1, 2, and 3
T_{Out1} / T_{Out2} / T_{Out3}	Fluid Outlet Temperatures for Collectors 1, 2, and 3

General Introduction

Solar energy is one of the most important and widely used sources of renewable energy in the world due to its significant role in reducing dependence on fossil fuels and minimizing the environmental pollution associated with conventional energy consumption. Among the technologies developed to utilize solar energy, flat-plate solar thermal collectors have attracted considerable attention because of their simple design, low cost, and suitability for a wide range of thermal applications such as water heating, air heating, and solar drying.

The history of solar collectors dates back to humanity's earliest attempts to harness solar radiation as a source of thermal energy. However, significant development in this field began during the nineteenth century. In 1767, the Swiss scientist Horace-Bénédict de Saussure invented the first simple solar box capable of collecting and retaining solar heat, which is considered one of the earliest prototypes of solar collectors. Later, in 1891, the American inventor Clarence Kemp patented the first commercial solar water heater, marking the beginning of the practical utilization of solar thermal energy.

Despite their advantages, conventional flat-plate solar collectors face several challenges and limitations, including high thermal losses, insufficient absorption efficiency, and a heavy dependence on the absorber surface's ability to transfer heat effectively to the working fluid. These factors can significantly reduce the overall thermal efficiency of the system. Consequently, improving the heat transfer characteristics of absorber surfaces has become one of the most crucial research areas in solar thermal engineering.

PROBLEM STATEMENT

Traditional flat absorber plates painted with standard matte black coatings often suffer from limited convective heat transfer rates to the working fluid due to the formation of a stagnant thermal boundary layer. While various surface modifications such as fins or corrugated plates have been investigated, they often increase manufacturing complexity and cost. Passive surface texturing using recycled metallic waste presents a promising, low-cost alternative to augment heat transfer area and induce local turbulence, yet the optimal density and thermal behavior of such composite surfaces require deeper experimental investigation.

OBJECTIVES OF THE WORK

To address this challenge, the primary objective of this Master's thesis is to experimentally evaluate the impact of surface roughness and extended surface areas on the thermal efficiency of flat-plate solar collectors. Specifically, this work investigates the integration of industrial aluminum shavings into the absorber surface. Three identical small-scale solar collectors were fabricated and tested under real climatic conditions: a reference collector with a standard black-painted flat plate, a second collector enhanced with 20 grams of aluminum shavings, and a third collector enhanced with 40 grams of aluminum shavings. By comparing their thermal performances, this study aims to determine the effect of shaving mass on heat gain and overall collector efficiency.

THESIS OUTLINE

To present this work clearly, the thesis is structured into three main chapters:

- **Chapter One** presents the general principles and fundamental concepts related to renewable energy, with a particular emphasis on solar thermal energy and the theory governing flat-plate solar thermal collectors.
- **Chapter Two** outlines the experimental methodology, detailing the step-by-step construction of the three flat-plate solar collectors, the materials used, the surface preparation process, and the experimental instrumentation.
- **Chapter Three** focuses on the presentation, discussion, and comparative analysis of the experimental results obtained during the testing period, highlighting the variation in fluid temperatures and calculated thermal efficiencies.

Finally, a general conclusion summarizes the key findings of this research and proposes recommendations for future work.

I-1 Introduction

Solar thermal energy stands as one of the most promising avenues among renewable resources due to its high geographic availability, clean operating profile, and technological scalability. Among the various engineering designs developed to capture this resource, Flat-Plate Solar Collectors (FPCs) are extensively utilized for low-to-medium temperature applications, such as domestic water heating, air heating, and industrial solar drying. However, the primary barrier to optimizing these systems lies within the fluid dynamics and heat transfer limitations at the absorber surface. Traditional plates often suffer from limited heat transfer rates to the working fluid due to the formation of a stagnant thermal boundary layer. This chapter establishes the foundational thermodynamic and aerodynamic principles governing flat-plate collectors. Furthermore, it provides a comprehensive review of prior literature focused on passive heat transfer enhancements, creating the necessary theoretical framework to evaluate the modification of absorber surfaces using particulate metallic roughness to mitigate surface heat losses and improve overall performance.

I.1.1. Literature Review on Solar Thermal Collector Optimization

The progressive depletion of conventional fossil fuel reserves, coupled with the escalating environmental degradation caused by greenhouse gas emissions, has intensified the global transition toward sustainable energy alternatives [1]. Among the various renewable energy resources available, solar energy represents one of the most abundant, clean, and accessible options to alleviate the current ecological crisis [2]. Statistical data compiled on a global scale underscores that the deployment of solar thermal technologies is expanding rapidly as nations seek to decarbonize their industrial and domestic sectors [3]. Solar thermal collectors serve as the primary engineering devices designed to capture incident solar flux and convert it into usable thermal energy for applications ranging from water heating to solar distillation systems [4].

The thermal efficiency of these systems is heavily dictated by the complex heat transfer mechanisms occurring simultaneously between the absorber plate, the internal air cavities, the transparent glazing covers, and the surrounding ambient environment [5]. Comprehensive evaluations of flat-plate solar collector systems indicate that their operational success relies heavily on minimizing heat loss while maximizing solar energy collection [6]. In this context, addressing the intermittent nature of solar availability requires integrating concentrating solar power technology and thermal storage configurations to balance energy supply and demand [7]. Such technological advancements are crucial for mitigating renewable power generation costs, making solar installations economically viable for broad applications [8]. Consequently, mastering the fundamental principles of renewable energy resources is essential for designing modern energy conversion devices [9].

To maximize heat absorption, the selection of surface coatings and materials remains a critical engineering focus within the core principles of solar engineering [10]. The development of high-performance systems depends on optimizing structural layouts to capture maximum solar energy throughout the year [11]. Research indicates that evaluating flat-plate solar collector performance with a coated and uncoated glass cover profoundly impacts the top loss coefficient, as an appropriate glazing cover acts as a radiation shield that traps long-wave thermal emissions [12]. Furthermore, utilizing a glass cover with antireflection surfaces provides distinct thermal advantages for solar heating systems by drastically reducing reflection losses and increasing the optical efficiency of the collector [13].

The optimization of radiative properties through advanced material science has further advanced the performance of flat-plate technologies, particularly through advanced spectrally selective coatings for solar thermal applications [14]. Investigating the thermal behavior of water flow in solar collectors allows researchers to understand fluid dynamics and heat removal factor variations under transient conditions [15]. To further elevate efficiency, recent studies focus on heat transfer enhancement in solar collector tubes using nanofluids, which alter the fluid density and thermal conductivity for better heat extraction [16]. These efforts are supported by comprehensive technical reviews of mid- to high-temperature solar selective absorber materials to ensure durability and high absorptivity [17].

A review of the latest advances on solar thermal collectors reveals that researchers are increasingly combining numerical modeling with experimental validation to assess component-level performance under transient environmental conditions [18]. Recent thermal performance investigations of flat-plate solar collectors have focused on optimizing internal geometries and minimizing heat loss [19]. These recent advances in solar thermal collectors and systems highlight a clear trend toward smart materials and structural enhancements [20]. Through sophisticated thermal performance analysis of solar collector components using numerical modeling, the detailed temperature distributions of the absorber, internal cavity air, and glazing covers can be mapped accurately over time [21]. These findings are supported by a performance analysis of solar thermal collectors in a comprehensive review that establishes a baseline for evaluating specialized variations of solar technology [22].

To evaluate practical improvements, a comparative experimental study of new absorbent surface coatings for flat plate solar collectors revealed that epoxy coating is highly suitable for system maintenance due to its ability to absorb solar energy at a rate of 4% to 6% compared to acrylic coating, while ensuring that it does not peel off at a rate exceeding 5%, which results in a significantly better thermal performance than other conventional types [23]. Beyond surface treatments, an experimental performance investigation of flat plate solar collectors based on contact materials evaluated the effect of the interface material placed between the absorber plate and the riser tube [24]. This study found that a water system functions better than dry or wet sand as an interface layer between the tubes and the plate because it effectively increases the contact area and improves the internal heat transfer coefficient, yielding 516 Watts of heat when thermal radiation reaches 504 Watts per meter squared [24].

These structural modifications are often integrated into hybrid photovoltaic-thermal systems, where selective coatings improve both electrical and thermal yields [25]. Similar optimization trends are observed in solar air heaters, where artificial roughness and coatings are reviewed to enhance convective heat transfer [26]. For specialized outdoor applications, understanding unglazed solar collectors performance is critical, as they interact directly with ambient wind conditions without the protection of a top glass cover [27]. To maintain hot water availability during off-sun hours, integrated collector storage solar water heaters are employed to combine collection and storage in a single unit [28]. Finally, analyzing photovoltaic-thermal systems performance reviews underscores the importance of cooling the electrical components while simultaneously extracting high-grade thermal energy [29].

The extensive literature surveyed demonstrates a clear and progressive evolution in the field of solar thermal engineering. Researchers have transitioned from analyzing standard baseline systems to developing highly sophisticated optimization strategies, which include advanced spectrally selective coatings, contact-resistance enhancements, internal geometric modifications, and specialized working fluids. However, while these individual advancements show significant promise for maximizing heat capture and minimizing thermal losses, a critical engineering need remains to evaluate how these modifications perform when integrated practically and cost-effectively into a unified system layout. Understanding these fundamental heat transfer constraints and material behaviors under real atmospheric conditions sets the necessary scientific baseline. Consequently, to fully grasp how these architectural optimizations influence fluid dynamics and thermal efficiency, it is first essential to establish the core thermodynamic principles that govern the conversion of solar radiation into usable thermal energy, as detailed in the following section.

I-2 Fundamentals of Solar Thermal Conversion

I-2-1 The Role of Renewable Energy and its Link to Solar Collectors

Renewable energy systems have emerged as a foundational pillars of modern engineering due to their capacity to provide sustainable, clean energy alternatives while significantly minimizing the greenhouse gas emissions (such as CO_2) and environmental pollution associated with conventional fossil fuels as shown in Figure I.1. By shifting reliance toward naturally replenishing, inexhaustible resources, these technologies mitigate climate change, reinforce energy security, and foster long-term economic stability [3].

Among these resources, solar energy holds a prominent position due to its exceptional abundance, geographical accessibility, and technical versatility. While photovoltaic systems directly convert solar photons into electricity, solar thermal energy conversion focuses on capturing this radiation to produce high-efficiency, clean heat.

The technical viability of these systems is intrinsically tied to regional solar potential. Algeria possesses one of the highest solar heritages in the world, particularly in its vast southern regions such as the cities of El Oued and Ouargla where the annual sunshine duration consistently exceeds 3,000 hours as shown in Figure I.1. This intense, prolonged exposure translates to an extraordinary solar flux density, positioning the country as an ideal landscape for large-scale solar thermal deployment [1], [2].

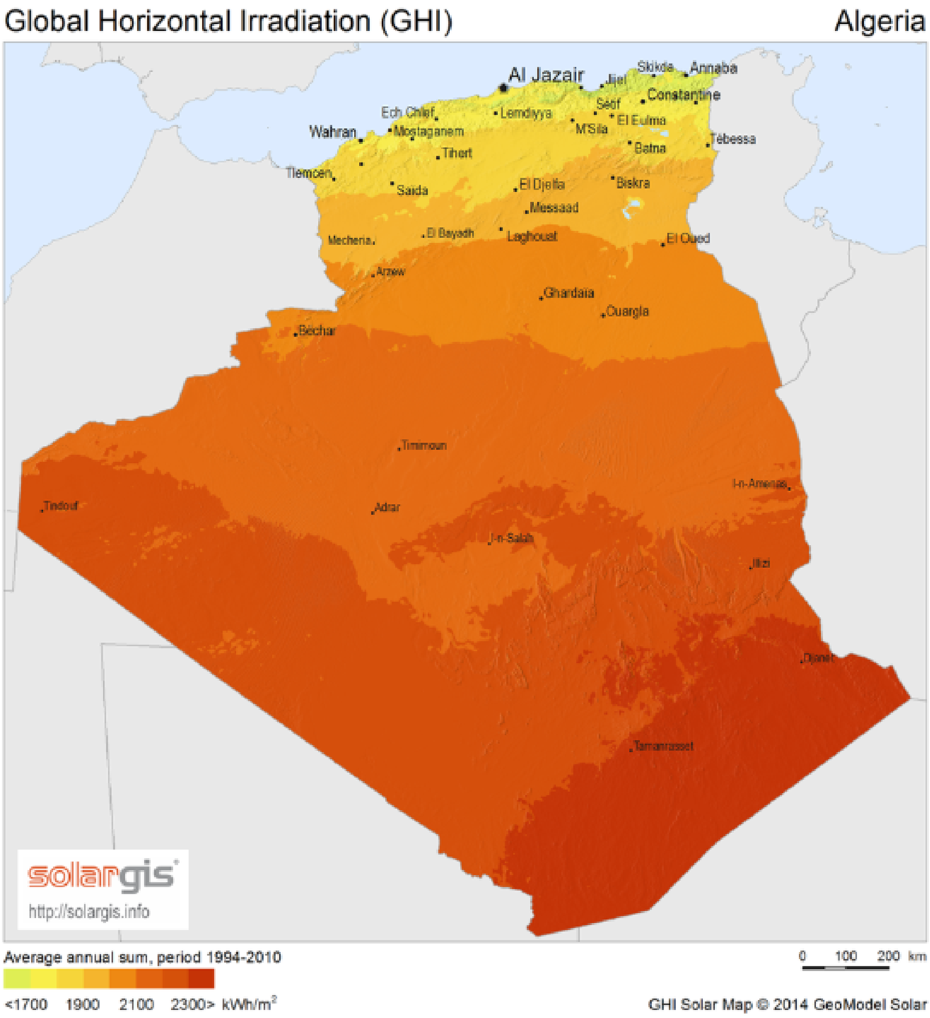

Figure I.1: Renewable energy

The direct operational link between raw solar availability and practical thermal utility is established by the solar thermal collector, which fundamentally acts as a specialized heat exchanger. These devices intercept incoming solar radiation, absorb its photon energy, and convert it into sensible heat. This generated thermal energy is immediately transferred to a working fluid typically water or air circulating through the system. The heated fluid can then either be routed directly to meet localized thermal demands or directed into thermal energy storage units to sustain operations during periods of low solar irradiance or nighttime conditions. Therefore, the solar collector serves as the critical primary mechanism for translating diffuse environmental radiation into useful, controllable thermal power.

I-2-2 Main Engineering Applications of Solar Thermal Energy

Solar thermal technology is highly adaptable, spanning a wide array of domestic, agricultural, and industrial applications based on the operating temperature thresholds required:

- Domestic Sector Applications
  In residential and commercial buildings, low-temperature solar collectors are commonly deployed to provide domestic hot water and space heating by utilizing incident solar radiation to warm indoor environments. Furthermore, solar thermal energy can be successfully integrated into building cooling configurations, where harvested solar heat serves as the primary thermal driving force for absorption chillers and thermally activated cooling processes, typically operating at temperature baselines up to approximately 70°C [4], [5].
- Agricultural Sector Applications
  Solar thermal systems are widely utilized for the dehydration and drying of agricultural products. This passive or active heating methodology accelerates moisture evaporation under controlled conditions, effectively preserving the nutritional quality, color, and long-term storage viability of the crops while preventing microbial spoilage [6].
- Industrial Sector Applications
  In medium-temperature brackets, solar thermal energy is increasingly harnessed for industrial process heat, including low-pressure steam production for the food processing industry and thermal water desalination frameworks. In desalination applications, solar thermal energy is used to heat and evaporate seawater or brackish water, separating pure water vapor from salts and contaminants before it is condensed into fresh, potable water [7].
- Utility-Scale Power Generation (CSP)
  In high-temperature applications, Concentrated Solar Power (CSP) plants employ massive engineered arrays of tracking mirrors or lenses to focus direct solar radiation onto a centralized thermal receiver, elevating localized temperatures significantly. This intense heat is transferred to a high-capacity working fluid, such as molten salt, which acts as a thermal energy storage medium. The stored energy is subsequently extracted to produce high-pressure steam, driving conventional steam turbines connected to electrical generators for large-scale power production [8].

I-3 Solar Thermal Collector

I-3-1 Definition of a Solar Collector

A solar thermal collector is a specialized thermodynamic heat exchanger designed to transform radiant energy from the sun into usable thermal energy. Unlike conventional heat exchangers that facilitate heat transfer between two or more flowing fluids, a solar collector captures incident electromagnetic solar radiation and converts it into internal thermal energy within an absorber material. This accumulated heat is subsequently transferred to a working fluid such as water, air, or a specialized thermal oil that circulates through the internal channels of the device. The heated fluid then transports this thermal energy either directly for immediate use or to a thermal storage system for later deployment in residential, agricultural, or industrial processes.

I-3-2 Operating Principle of Solar Thermal Conversion

The fundamental operating principle of a solar thermal collector relies on the laws of thermodynamics, specifically involving radiation absorption, conduction, and convection. The conversion process occurs through the following sequential stages:

- **Radiation Absorption**
  Incident shortwave solar radiation passes through any transparent glazing layers and strikes the absorber surface. This surface is engineered to possess a high absorptivity coefficient, allowing it to capture the vast majority of the incoming photons and convert their electromagnetic energy into sensible heat, rapidly elevating the temperature of the absorber plate.
- **Thermal Conduction**
  The heat accumulated within the absorber plate is transferred via molecular conduction across the plate material toward the outer walls of the fluid conduits or riser tubes. To maximize this heat transfer rate, the absorber and tubes are fabricated from materials with high thermal conductivity, such as copper or aluminum, ensuring minimal thermal resistance at the physical interface.
- **Convective Fluid Heating**
  As the working fluid circulates through the riser tubes, heat is transferred from the hot inner tube walls to the fluid via forced or natural convection. This mechanism causes a steady enthalpy increase along the flow path, resulting in the progressive rise of the fluid temperature from the inlet toward the system discharge.

I-3-3 Classification and Types of Solar Collectors

Solar collectors are broadly categorized based on their mechanical design, optical configuration, and the operating temperatures they can achieve. They are generally classified into non-concentrating and concentrating systems:

I-3-3-1 Non-Concentrating Collectors (Low-to-Medium Temperature Systems)

Flat-Plate Collectors (FPC)

These are the most common non-concentrating devices utilized for low-to-medium temperature applications, typically ranging from 30 to 80 degrees Celsius as shown in Figure I.2. They feature a large, flat absorber area that captures both direct and diffuse solar radiation simultaneously. Because the geometric area capturing the solar flux is identical to the absorbing area, these systems do not require tracking mechanisms and are highly reliable, cost-effective, and durable for domestic water heating and low-temperature solar distillation.

Figure I.2: Flat-plate solar collector

Evacuated Tube Collectors (ETC)

Unlike flat-plate configurations that rely on a single, continuous flat casing, the Evacuated Tube Collector (ETC) features a modular structural layout composed of multiple parallel rows of individual glass tubes connected to a central header manifold as shown in Figure I.3. Each modular element is constructed using a double-walled concentric tube design made from heavy-duty borosilicate glass. During the manufacturing process, the air contained within the annular space between the outer and inner glass tubes is mechanically evacuated, creating a high-grade, permanent thermal vacuum.

From a thermodynamic standpoint, this vacuum layer serves as an almost near-perfect insulation barrier. Because conduction and convection require a physical material medium to transfer kinetic energy between molecules, the total elimination of air molecules within the annular cavity completely suppresses these two primary heat loss mechanisms ($Q_{cond} \approx 0$ and $Q_{conv} \approx 0$). Consequently, the only path remaining for heat to escape from the inner tube back to the ambient environment is through long wave thermal radiation, which is strictly managed using advanced surface treatments.

Figure I.3: Evacuated tube collector

Unglazed Solar Collectors

Unglazed solar collectors are the most simplified and economical type of non-concentrating solar thermal technology as shown in Figure I.4. They consist entirely of a bare absorber plate made from UV-stabilized polymers, such as plastic or rubber, or low-cost extruded metals like aluminum. Unlike standard solar panels, they completely lack a top transparent glass cover and have no rear thermal insulation backing, allowing the working fluid to flow through channels that are directly exposed to the outside air. Because there is no protective glass layer, these collectors interact directly with ambient weather conditions and are highly susceptible to convective heat losses caused by blowing wind, which rapidly strips heat away from the bare surface.

Despite losing heat quickly at higher temperatures, unglazed collectors are remarkably efficient for low-temperature applications. Since sunlight does not have to pass through a glass cover, there are zero reflection or optical losses, allowing the bare material to absorb a massive amount of solar energy. When the required fluid temperature is kept very close to the ambient air temperature, the heat loss to the surrounding wind drops to near zero. Because they are cheap to manufacture, easy to install, and require minimal maintenance, unglazed solar collectors are the perfect engineering choice for low-temperature needs, such as heating swimming pools, preheating industrial process water, and drying agricultural crops.

Figure I.4: Unglazed collector

I-3-3-2 Medium-Concentrating Collectors (Intermediate Temperature Systems)

Compound Parabolic Collectors (CPC)

Compound Parabolic Collectors (CPC) are non-imaging concentrating solar systems that bridge the gap between flat-plate and high-concentrating technologies as shown in Figure I.5. They utilize carefully curved, parabolic reflective walls shaped like a funnel to collect and direct incident sunlight onto a centrally located absorber tube.

The primary engineering advantage of the CPC design is its wide acceptance angle. This unique optical characteristic allows the collector to capture not only direct sunlight but also a substantial portion of diffuse solar radiation that has been scattered by clouds of dust. Because of this wide angle of view, the system can operate at high thermal efficiencies throughout the day without the need for complex, expensive automatic solar tracking systems. This makes CPCs a highly reliable and cost-effective solution for mid-temperature applications like industrial process heating and solar cooling.

Figure I.5: Compound parabolic collectors

Linear Fresnel Reflectors (LFR)

This technology utilizes long, thin rows of flat or slightly curved mirrors mounted at ground level as shown in Figure I.6. These reflective strips are independently adjusted to track the sun and focus the incident solar beams onto a single, elevated stationary linear receiver tube running parallel above the mirror field. LFR systems are increasingly favored in industrial process heat applications due to their simplified structural design and lower capital cost compared to curved parabolic troughs.

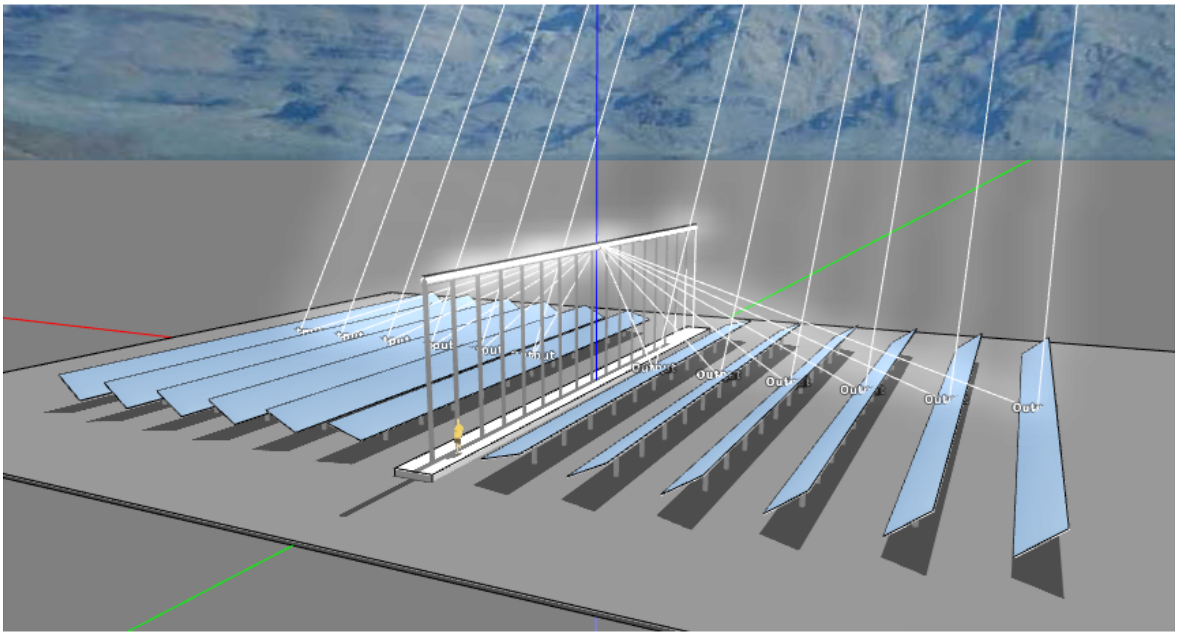

Figure I.6: Linear Fresnel Reflectors

I-3-3-3 High-Concentrating Collectors (High-Temperature Systems)

A Parabolic Trough Collectors (PTC):

Parabolic Trough Collectors utilize long, parabolic ally curved sheet mirrors to focus direct solar radiation onto a linear receiver tube positioned precisely along the focal line of the trough as shown in Figure I.7. To minimize thermal losses at elevated temperatures, the receiver tube is typically enclosed within an evacuated glass sleeve. PTC systems require a single-axis solar tracking mechanism to follow the sun from east to west, allowing them to heat thermal oils or steam up to 400 degrees Celsius for industrial processing and commercial electricity generation.

Figure I.7: Parabolic trough collectors

Parabolic Dish Collectors

These systems feature a large, bowl-shaped parabolic concentrator that tracks the sun across two axes to focus solar radiation onto a single focal point as shown in Figure I.8. A compact thermal receiver is mounted at this focal spot to absorb the highly concentrated energy. Because of the extremely high concentration ratios achieved, these systems can generate temperatures exceeding 700 degrees Celsius. They are often coupled directly with a localized Sterling engine at the focal point to convert the thermal energy immediately into electricity.

Figure I.8: Parabolic dish collectors

Solar Power Towers (Central Receiver Systems)

Central receiver systems utilize a vast field of large, computer-controlled, dual-axis tracking mirrors called heliostats as shown in Figure I.9. These mirrors continuously track the sun and reflect direct solar radiation onto a single, large receiver mounted at the top of a centrally located tower. By concentrating energy from thousands of flat mirrors onto a single point, operating temperatures can exceed 1000 degrees Celsius. This high-grade heat is transferred to a working fluid, such as molten salt, which can store the thermal energy for high-efficiency steam turbine power generation during off-sun hours.

Figure I.9: Solar power towers

I-4 Flat-Plate Solar Collector (FPC) Architecture

I-4-1 Definition and Structural Layout

The Flat-Plate Solar Collector is a specialized non-concentrating solar thermal device engineered to operate within low-to-medium temperature ranges as shown in Figure I.10. Structurally, it is designed as a compact, layered assembly housed within a rigid, protective exterior casing. The primary function of this structural configuration is to hold all internal thermodynamic components securely in place, protect them from harsh environmental weathering such as rain, sandstorms, and ambient humidity and maintain a sealed internal cavity that minimizes unwanted thermal energy dissipation.

The overall structural layout consists of an external metal or composite frame, inside of which thick layers of rear and side insulation are placed to eliminate conductive heat leakage. Directly above the insulation sits the fluid circulation network, which is mechanically bonded to the main metallic absorber plate. The entire assembly is sealed from above by a high-transmittance transparent glazing cover. This layered arrangement ensures that as direct and diffuse solar rays strike the collector surface, the captured energy is efficiently channeled into the working fluid with minimal optical or thermal losses. Furthermore, the structural layout dictates the fluid dynamics of the system, where fluid enters through a bottom header manifold, distributes evenly across multiple parallel riser tubes to extract heat from the absorber, and collects at a top header manifold before exiting the system at an elevated thermal state. Figure I.4 represents a flat solar collector and its cross-section.

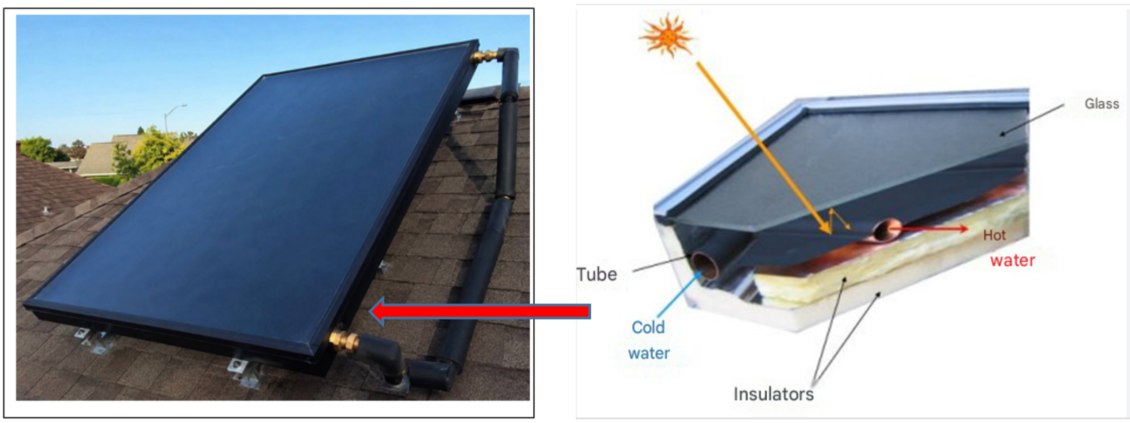

Figure I.10: Flat-plate solar collector

I-4-2 Core Physical Components

a) Transparent Glazing Cover

The transparent cover forms the uppermost layer of the collector assembly and acts as an optical filter. Its primary function is to permit maximum transmission of shortwave solar radiation (typically within the wavelength range of 0.3 to 3.0 micrometers) to reach the absorber plate beneath it. Concurrently, it suppresses thermal energy losses via two distinct mechanisms:

- Convective Suppression: It creates a stagnant air gap above the absorber plate, minimizing convective heat losses driven by ambient wind across the collector surface.
- Radiative Trapping (The Greenhouse Effect): Standard glass exhibits high opacity to long wave infrared thermal radiation (above 3.0 micrometers) re-emitted by the heated absorber plate, effectively trapping the thermal energy within the collector core.

However, its operational performance can be degraded by environmental factors such as dust accumulation, salt deposition, and incorrect orientation angles, all of which reduce optical transmittance and induce reflective losses.

b) Absorber Plate

The absorber plate is the critical thermodynamic engine of the flat-plate collector. Positioned directly beneath the glazing, its objective is to capture the transmitted solar photons and convert them into localized sensible heat. To optimize performance, traditional absorber plates are fabricated from highly conductive metals (such as copper or aluminum) and treated with selective surface coatings. These specialized coatings are designed to exhibit high solar absorptivity $\alpha = 0.95$) coupled with a very low thermal emissivity $\varepsilon = 0.12$), significantly reducing radiative heat re-emission back to the glass cover.

From a fluid dynamics perspective, a major limitation of standard flat absorber surfaces is the formation of a stagnant thermal boundary layer in the fluid flowing over or near the plate. This boundary layer acts as an insulating barrier, restricting the rate of convective heat transfer from the metallic matrix to the circulating fluid.

c) Fluid Flow Channels / Riser Tubes

The riser tubes or flow channels are structurally bonded to or integrated within the absorber plate to facilitate the continuous transport of the generated heat. Conductive energy from the absorber plate propagates laterally toward these channels, where it is transferred via forced or natural convection to the circulating working fluid (such as water or air).

An optimized design relies on a multi-channel network rather than a single large conduit. This configuration distributes the fluid flow uniformly across the plate area, eliminating localized hot spots, ensuring a homogeneous temperature gradient, and maximizing the heat removal factor. Structural bonding between the plate and the tubes must exhibit negligible thermal contact resistance; any mechanical separation, corrosion, or scale deposition within the tubes severely disrupts the thermal transport loop.

d) Back and Side Thermal Insulation

To prevent the dissipated heat from escaping through the sides and bottom of the collector housing, thick layers of high-resistance thermal insulation are installed. Materials with low thermal conductivity, such as glass wool, rock wool, or polyurethane foam, are fitted tightly beneath the riser tube network and along the inner perimeter of the casing. Effective insulation design ensures that conductive leakage to the external environment is minimized, forcing the vast majority of the captured energy to remain locked within the working fluid matrix.

e) Outer Enclosure / Casing

The outer casing serves as the structural framework that seals and protects the internal mechanical and optical components. Fabricated from rigid, weather-resistant materials such as extruded aluminum alloys, galvanized steel, or heavy-duty polymers, it shields the insulation and absorber plate from mechanical impacts, moisture infiltration, and wind forces. Additionally, a properly sealed casing prevents cold ambient air leakage into the collector core, maintaining structural stability and preserving the internal thermal baseline of the system.

I-4-3 Engineering Advantages and Disadvantages of Solar Thermal Energy

The detailed thermodynamic and engineering evaluation presented in Table I.1 underscores the complex balance between high thermal performance and operational constraints that define modern solar thermal technology. From a thermodynamic perspective, the primary advantage of flat-plate solar collectors lies in their direct energy conversion mechanism. Unlike photovoltaic panels, which must convert photon energy into electrical current before it can be converted back into heat introducing substantial conversion losses along the way thermal collectors absorb incident electromagnetic shortwave radiation and transform it directly into sensible heat within the lattice structure of the absorber plate. This streamlined energy path allows the system to achieve remarkably high thermal efficiencies, often operating between 60% and 70% under peak solar insolation.

Furthermore, because these non-concentrating collectors utilize a static mechanical layout devoid of moving parts, they are highly reliable, experiencing virtually no mechanical wear, which drastically minimizes long-term operational and maintenance expenditures. When coupled with high-capacity Thermal Energy Storage (TES) systems, such as insulated water tanks or phase-change materials, these collectors can successfully store excess midday heat and discharge it during off-sun hours, effectively transforming an intermittent resource into a predictable, dispatch able thermal supply that can directly displace fossil fuels in domestic and industrial operations.

However, transitioning this technology from a theoretical thermodynamic ideal to a rugged, field-deployed system introduces significant engineering trade-offs and vulnerabilities. The most critical operational challenge is the system's absolute vulnerability to meteorological intermittency and extreme environmental conditions. Because the heat transfer rate depends heavily on the temperature gradient between the hot absorber plate and the ambient air, convective and radiative heat losses escalate sharply as the collector heats up. This fundamental thermodynamic limitation restricts flat-plate configurations strictly to low-and-medium temperature applications, as operating at higher temperatures causes thermal efficiency to drop significantly.

Additionally, field installations face severe environmental risks; in cold climates, sub-zero ambient temperatures can freeze the internal working fluid, causing volumetric expansion that can easily rupture copper riser tubes. Conversely, during periods of high solar radiation coupled with zero fluid flow a condition known as stagnation the internal cavity can reach extreme temperatures, causing fluid boiling, pressure spikes, and the thermal outgassing of insulation materials. Managing these dual risks requires sophisticated engineering interventions, such as integrating glycol-based antifreeze loops, pressure-relief valves, and automated drain-back systems, which inevitably increases the initial capital expenditure and complexity of the solar installation.

Table I.1: Detailed Thermodynamic and Engineering Evaluation of Solar Thermal Energy

Category	Core Technical Factor	Thermodynamic & Engineering Mechanism	Practical Impact on System Operation	Design Optimization Solutions
Engineering Advantages	High Direct Conversion Efficiency	Avoids intermediate energy transformation steps; photons directly excite the lattice structure of the absorber plate to generate sensible heat.	Achieves operating efficiencies of 60% to 70%, far outperforming photovoltaic systems for thermal applications.	Use of high-conductivity substrate materials (copper or aluminum) and high-absorptivity selective coatings.
	Decarbonization & Sustainability	Zero operational combustion; replaces fossil fuel utilization directly at the thermal demand source.	Drastically lowers carbon dioxide, nitrogen oxides, and greenhouse gas footprints for domestic and industrial plants.	Scale up collector field areas to substitute heavy fuel or natural gas-fired industrial boilers.
	Minimal Operational Costs	Static mechanical configuration eliminates moving parts, reducing mechanical friction, wear, and structural fatigue.	Results in exceptionally low long-term operating expenditures and extended system lifespans.	Use of low-iron tempered glass and UV-stabilized casing materials to resist environmental weathering.
	Thermal Energy Storage (TES) Integration	Captures excess thermal energy via sensible or latent heat storage materials during peak radiation periods.	Mitigates solar intermittency by shifting energy delivery to cloudy periods or night hours.	Incorporating well-insulated hot water storage tanks or phase-change material (PCM) matrices.
Engineering Disadvantages	Meteorological Intermittency	Solar flux varies dynamically based on the solar zenith angle, cloud cover, and seasonal variations.	Creates a critical mismatch between peak energy collection (midday) and peak user demand (morning/evening).	Implementation of automated auxiliary backup heaters and smart differential temperature controllers.
	Upfront Capital Expenditure	Requires high-purity raw materials (copper, selective coatings, optical glass) and specialized plumbing infrastructure.	Extends the financial payback period, which can deter initial industrial or residential adoption.	Standardizing manufacturing layouts and optimizing fluid flow rates to maximize specific energy yields.
	High-Temperature Thermal Losses	Radiative and convective heat dissipation scales sharply as the temperature gradient between the absorber and ambient air grows.	Restricts non-concentrating flat-plate collectors strictly to low-and-medium temperature operations.	Employing advanced spectrally selective coatings with low thermal emissivity and high-vacuum enclosures.
	Freezing and Stagnation Risks	Low ambient temperatures cause fluid freezing and volumetric expansion; zero-flow state under high solar flux causes boiling.	Freezing ruptures internal riser tubes; high stagnation temperatures cause fluid boiling and insulation outgassing.	Using glycol-water antifreeze mixtures, automated drain-back configurations, and pressure-relief valves.

I-5 Conclusion

This introductory chapter highlights the vital role that solar thermal technologies play in our transition to clean, renewable energy. By examining how solar collectors are built, how they manage heat transfer, and how they have evolved over time, this review successfully connects basic engineering theory to real-world energy solutions.
Ultimately, the comprehensive insights and theoretical baselines established throughout these sections provide the exact foundational knowledge needed to summarize the core findings of this chapter and support the upcoming experimental phases of this research.

The core findings and theoretical baselines established in this chapter are summarized through the following key points:

- **Foundational Framework Established**
  The global energy landscape demands a rapid transition toward sustainable alternatives, highlighting solar energy conversion as a clean, reliable solution to substitute conventional fossil fuels and directly reduce greenhouse gas emissions.
- **Evolution of the Technology**
  The historical development of solar installations demonstrates a clear academic shift over time, showing that collector optimization has transitioned from basic empirical testing toward advanced material science, specialized selective coatings, and precise fluid dynamics tuning.
- **Technology Selection**
  While high-concentrating tracking systems are necessary to achieve the elevated temperatures required for industrial power generation, non-concentrating flat-plate collectors remain the most durable, reliable, and cost-effective option for low-to-medium temperature applications.
- **Selection of the Experimental Prototype**
  Based on the specific low-to-medium temperature operational requirements, structural reliability, and economic viability analyzed in this review, **the flat-plate solar collector (FPC) configuration has been strictly selected as the primary experimental prototype for this Master's thesis.** This classic geometry serves as the baseline system upon which our custom design modifications and thermal enhancements will be physically implemented, tested, and analyzed in the subsequent experimental phases.
- **Component Optimization**
  The overall thermal efficiency of a flat-plate collector depends entirely on the design of its physical layers, requiring a balance between high-transmittance glazing covers to trap heat and high-absorptivity, low-emissivity selective coatings to minimize radiative losses.
- **Thermodynamic Trade-offs**

Real-world deployment reveals that while solar thermal conversion offers exceptional direct efficiency and low operating costs, it is fundamentally constrained by meteorological intermittency, as well as critical operational risks like fluid freezing and high-temperature stagnation.

- **Research Baseline Secure**
  Ultimately, the comprehensive insights gathered in this chapter establish the essential engineering context and theoretical baseline required to support the specific experimental configurations, data analysis, and structural modifications presented in the upcoming chapters of this thesis.

II-1 Introduction

This chapter represents the core empirical stage of the study, focusing on the experimental investigation aimed at evaluating the thermal performance of flat-plate solar collectors. In this work, a comparative analysis is conducted on three uniquely treated absorber surfaces operating simultaneously under identical environmental and operating conditions. This chapter provides a detailed description of all components of the experimental setup, including the geometric configuration of the collectors, the airflow mechanism designed within the system, and the thermal insulation techniques employed to minimize external heat losses. In addition, it presents the technical specifications of the measurement instruments used and outlines the systematic experimental procedure followed to ensure accurate, repeatable, and reliable data collection.

II-2 Description of the Experimental Work

The empirical testing and data collection were carried out adjacent to the Technological Hall of the Faculty of Technology (Mechanical Engineering Department) at the University of El Oued, Algeria, as illustrated in Figure II.1. The experimental site is situated within the southeastern region of the Algerian Sahara, characterized by specific geographic coordinates: a latitude of approximately 33.3561 degrees N, a longitude of 6.8632 degrees E, and an altitude of roughly 70 meters above sea level.

The complete experimental setup comprises three separate, small-scale flat-plate solar collectors designed to operate simultaneously under identical meteorological and boundary conditions. This simultaneous testing approach is strictly maintained to isolate and accurately compare the independent effect of the absorber plate surface modification on overall thermal performance.

The outdoor experimental trials were conducted daily from 08:00 to 16:00 over a period of three consecutive clear days, during which the aperture areas of the collectors were directly exposed to ambient solar irradiance. To maximize daily solar energy capture and minimize reflective losses, the three collectors were securely mounted on a testing rack facing due South, positioned at a fixed inclination angle equal to the localized latitude of El Oued (approximately 33 degrees).

Figure II.1: Location of the experimental testing site

II-3 Design, Dimensions, and Material Specifications of the Collectors

II-3-1 Structural Frame and Casing

To ensure a rigorous comparative study, three geometrically identical flat-plate solar collectors were constructed using standard workshop fabrication techniques as shown in Figure II.2. Every structural, material, and optical parameter was kept completely uniform across all three units to eliminate any geometric or material bias during data analysis. A key engineering objective of this assembly was the integration of accessible, locally sourced materials, demonstrating a sustainable, resilient, and cost-effective approach to solar thermal optimization in the region.
The outer enclosure of each solar collector was fabricated with precise square dimensions to establish a uniform surface envelope and ensure identical volume boundaries for the air stream. High-density wood was selected for the outer frame due to its low structural thermal conductivity, which helps minimize parasitic edge losses. The physical specifications of each individual enclosure are detailed below:

- Internal Length: 30 cm (300 mm)
- Internal Width: 30 cm (300 mm)
- Total Clear Aperture Area: 0.09 square meters per collector

To facilitate proper fluid transport through the systems, dedicated flow ports were drilled on opposite edges of each casing frame. One side serves as the air inlet manifold, while the opposing side acts as the fluid outlet manifold. This positioning ensures a cross-flow configuration across the absorber plate. The internal corners, joints, and perimeter lines of the wooden casings were thoroughly sealed using high-temperature thermal silicone to prevent ambient air infiltration or unwanted localized leakage, which could distort mass flow calculations.

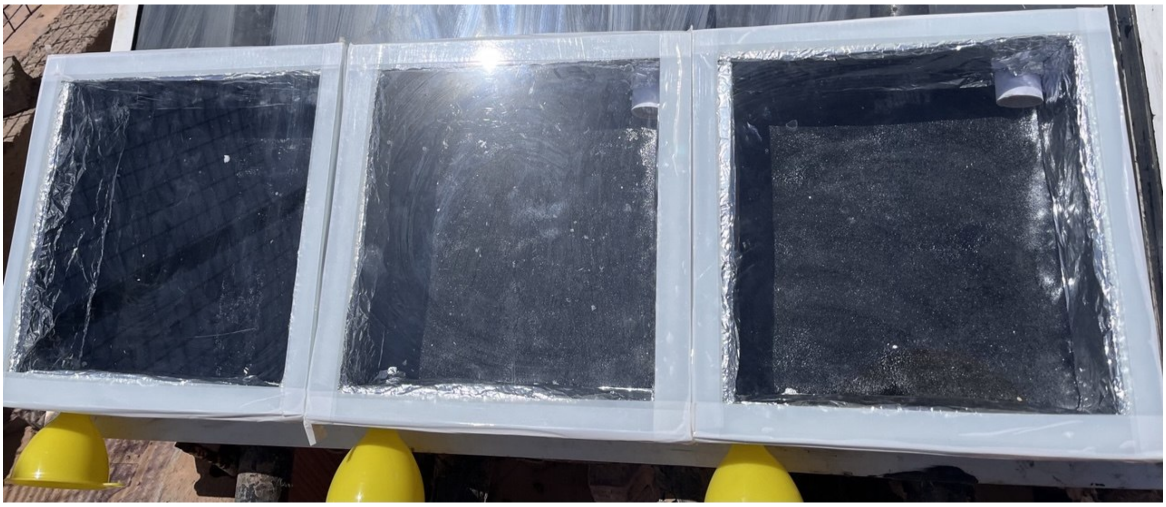

Figure II.2 : Assembled structural frames of the three flat-plate solar collectors

II-3-2 Thermal Insulation Layer

To suppress conductive heat dissipation through the rear and side walls of the devices, a high-resistance thermal insulation strategy was applied using widely available local insulation products. The inner surfaces of each collector housing were fully lined with polystyrene insulation sheets covered with a reflective layer of aluminum foil as shown in Figure II.3.

This composite insulation serves a dual purpose: the dense polystyrene core acts as a primary barrier to minimize conductive heat loss through the bottom and sides, while the bright aluminum sheet reduces radiative heat transfer by reflecting internal infrared radiation back toward the absorber matrix. Additionally, this aluminum layer increases the material's resistance to environmental effects and thermal degradation over time.

By maintaining identical insulation materials, thicknesses, and geometric layouts across all tested collectors, uniform operating conditions were strictly established. This eliminates localized thermal losses as a variable, ensuring that the overall heat loss coefficient of the collector shell remains constant and enabling an accurate, objective comparison where the only variable considered is the absorber surface properties.

Figure II.3: Internal lining displaying the polystyrene insulation layer layered with protective aluminum foil

II-3-3 Transparent Glazing Cover

A single layer of highly transparent commercial glass was positioned at the top of each collector frame to shield the internal core and trap incoming energy as shown in Figure II.4. The glazing parameters are established as follows:

- Glass Composition: Standard clear float glass

- Glass Sheet Thickness: 5 mm

The glass cover is securely mounted using tight rubber profiles to prevent direct glass-to-frame thermal bridging. This transparent cover creates a sealed air gap above the absorber plates, minimizing convective heat losses driven by ambient wind while establishing a localized greenhouse effect within each collector box by trapping long wave thermal radiation.

Figure II.4 : Explicit view of the 5 mm transparent glass covers prepared for installation

II-3-4 Absorber Surface Configurations

To systematically investigate the impact of artificial surface texturing on heat transfer enhancement, three distinct absorber surface configurations were prepared as shown in Figure II.5. Table II.1 summarizes the thermophysical properties of the materials used in the fabrication of the experimental flat-plate solar collector. The reported values were obtained from standard engineering references and published literature [30-32] and are representative of the materials used in this study. While the geometric dimensions of the metal plates remained perfectly identical at 30 cm by 30 cm, the surface morphology of each plate was altered to establish a clear comparative matrix:

- Configuration A (Reference Baseline):
  This configuration consists of a standard, smooth metal plate coated uniformly with a matte black-tinted paint. It contains no structural or material modifications, serving as the experimental control line to establish the baseline efficiency of a traditional flat-plate collector.
- Configuration B (20g Aluminum Powder Matrix):
  This surface was modified by uniformly distributing and bonding exactly 20 grams of fine aluminum powder across the 30 cm by 30 cm metal plate before applying the final matte black coating. This configuration introduces a controlled layer of micro-roughness designed to induce localized fluid mixing in the adjacent air stream.
- Configuration C (40g Aluminum Powder Matrix):
  This surface follows the exact same preparation protocol as Configuration B, but utilizes a mass of exactly 40 grams of aluminum powder. By doubling the mass density

of the metallic particles, this configuration creates a highly dense, packed arrangement of surface irregularities, maximizing both the effective heat transfer area and the path tortuosity for the moving air.

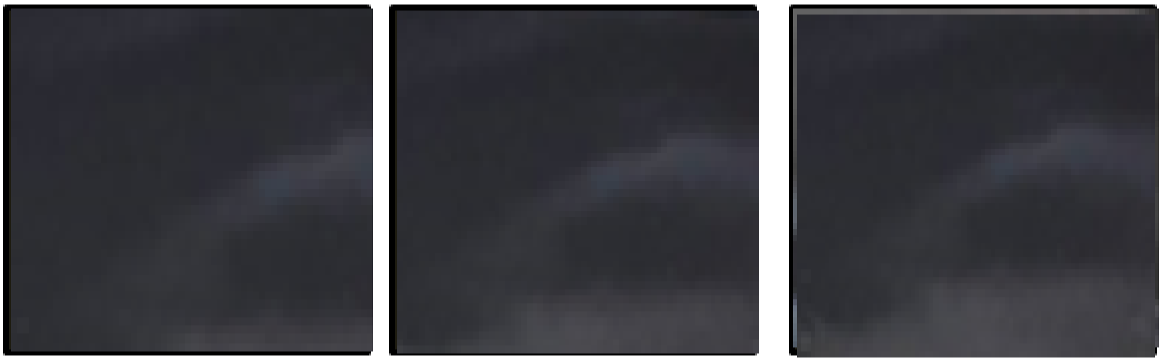

Figure II.5 : Prepared absorber plates showing the distinctive surface texture variations under the matte black coating

Table II.1 Thermophysical properties of the collector material [30-32]

Component	Material	Density (kg/m^3)	Thermal Conductivity (W/m·K)	Specific Heat (J/kg·K)	Emissivity
Collector frame	Wood (Pine)	500	0.12	1700	0.90
Transparent cover	Clear Float Glass	2500	1.05	750	0.88
Absorber plate	Aluminum	2700	205	900	0.09 (polished)
Insulation	Expanded Polystyrene (EPS)	20	0.034	1300	—
Reflective layer	Aluminum foil	2700	237	900	0.04

II-4 Airflow Management and Operational Testing Modes

To comprehensively evaluate the heat transfer enhancement induced by the modified absorber surfaces under different aerodynamic behaviors, the experimental campaign was divided into two distinct operating modes: natural convection (passive operation) and forced convection (active operation). This dual-mode approach allows for a direct thermodynamic comparison of how the aluminum powder micro-roughness affects the convective heat transfer coefficient under both buoyancy-driven and pressure-driven flow regimes.

II-4-1 Natural Convection Mode (Passive Operation)

During the initial phase of the experimental testing, the system was operated entirely as a passive solar air heater to evaluate performance under low-velocity conditions as shown in Figure II.6.

- **Flow Mechanism:** In this configuration, all mechanical ventilation components were deactivated or detached from the flow ports. The movement of air through the 30 cm by 30 cm collectors relied exclusively on the principle of natural buoyancy, commonly referred to as the thermosyphon effect.
- **Thermodynamic Behavior:** As solar irradiance penetrates the 5 mm glass cover and is absorbed by the matte black plates, the temperature of the air layer directly adjacent to the absorber surfaces rises rapidly. This localized heating causes the air to expand, reducing its density. The lighter, heated air naturally ascends along the inclined collector channel and exits through the upper outlet manifold. Concurrently, cooler and denser ambient air is drawn into the system through the lower inlet ports to maintain continuous, self-sustained fluid circulation.

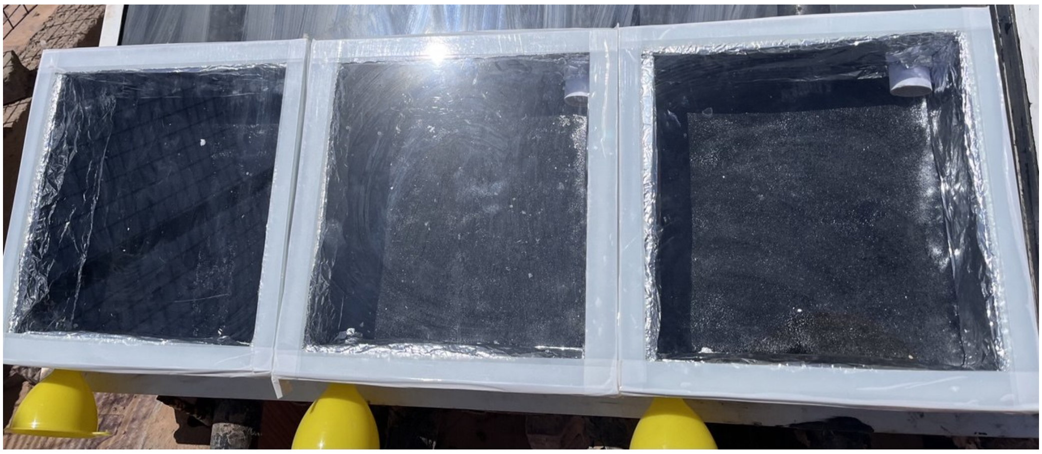

Figure II.6: Natural convection testing mode

II-4-2 Forced Convection Mode (Active Operation)

In the second phase of the investigation, the experimental setup was modified to operate under an active regime to assess the impact of controlled, higher-velocity air streams as shown in Figure II.7.

- **Flow Mechanism:** For this testing mode, mechanical ventilation fans were securely connected to the system's manifolds to mechanically force a steady stream of ambient air through the internal channels of the three collectors simultaneously.
- **Hydrodynamic Behavior:** The introduction of mechanical ventilation transitions the internal fluid dynamics from a slow, buoyancy-driven laminar flow to a pressure-driven flow with higher Reynolds numbers. Forcing the air stream across the irregular surface topographies of the 20g and 40g aluminum powder matrices promotes localized flow separation and reattachment. This artificial turbulence continuously breaks down the thick thermal boundary layer that typically forms over smooth plates, significantly increasing the rate of heat removal from the absorber to the working fluid.

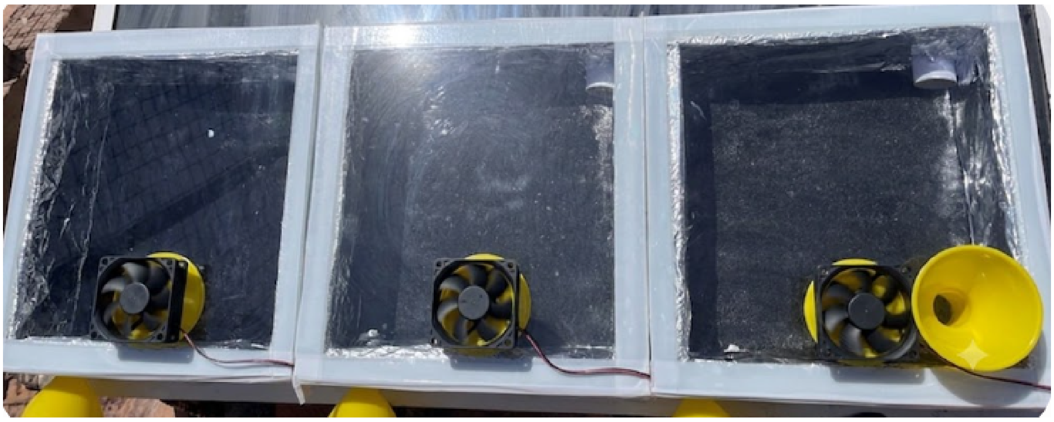

Figure II.7: Forced convection testing mode

II-5 Measuring Instruments

II-5-1 Temperature Measurement (Thermocouples)

Temperature monitoring across various critical points of the experimental solar collectors was achieved using calibrated thermocouples (typically Type-K or Type-T, depending on the specific model used) as shown in Figure II.8.

- **Sensor Placement:** Multiple sensors were permanently fixed to key components of each collector system to map the thermal gradient. These included sensors attached directly to the back of the reference, 20g, and 40g absorber plates, sensors placed on the external glass covers, and sensors positioned inside the inlet and outlet manifolds to measure the temperature rise of the working air stream.
  - **Data Recording:** All thermocouple wires were connected to a centralized digital multi-channel data logger (or digital handheld thermometers) to record temperature fluctuations at fixed time intervals (e.g., every 30 minutes) from 08:00 to 16:00.

Figure II.8: Thermocouples

II-5-2 Solar Radiation Measurement (Pyranometer)

To quantify the total available energy striking the aperture area of the collectors, a digital pyranometer was employed as shown in Figure II.9.

- **Operation and Alignment:** The pyranometer was mounted on the exact same testing rack as the solar collectors, maintaining the identical fixed inclination angle of 33 degrees facing due South. This alignment ensures that the measured global solar intensity (expressed in Watts per square meter, W/m²) corresponds exactly to the real flux incident on the 5 mm glass covers.
- **Application:** The hourly solar irradiance data collected by this instrument serves as the fundamental input variable for calculating the thermal efficiency curves of each configuration.

Figure II.9: Pyranometer

II-5-3 Air Velocity Measurement (Anemometer)

To monitor and regulate the hydrodynamic behavior of the working fluid inside the channels, a high-sensitivity digital anemometer was utilized.

- **Application in Natural Convection:** In the passive testing mode, the anemometer was used to verify the low-velocity exit air streams induced by the thermal buoyancy effect at the outlet ports.
- **Application in Forced Convection:** In the active testing mode, the anemometer was placed directly at the inlet or outlet manifolds to precisely measure the forced air velocity (expressed in meters per second, m/s). This velocity data is critical for calculating the mass flow rate of the air and determining the Reynolds number of the flow loop.

Figure II.10: Anemometer

II-6 Experimental Procedure and Fabrication Steps

The execution of this study was divided into two sequential phases: the physical fabrication and surface modification of the solar collectors in the workshop, followed by the systematic operational procedure during the outdoor experimental testing campaign. This structured approach was strictly followed to ensure that all modifications were uniform and that the data collection was rigorous and repeatable.

II-6-1 Preparation and Modification of the Absorber Plates

The modification of the absorbent surfaces was carried out step by step using manual techniques of bonding aluminum powder to the absorbent surfaces with black paint, as illustrated in Figure II.11. This crucial process is described below: This critical process is outlined below:

1. **Mechanical and Surface Cleaning:** Three identical 30 cm by 30 cm metallic sheets were selected. To ensure strong adhesion of the modification materials, each plate was treated with an organic solvent to degrease the surface and remove manufacturing oils.

The sheets were then mechanically sanded using fine-grit emery paper to remove dust and surface oxidation, creating a clean, raw metallic substrate.

2. **Weighing the Metallic Particles:** A high-precision digital laboratory scale was used to accurately measure two separate quantities of local aluminum powder: one sample of exactly 20 grams for Collector 2, and a second sample of exactly 40 grams for Collector 3.
3. **Application of the Adhesive Binder:** A thin, highly uniform layer of a high-temperature, heat-resistant adhesive binder was brushed onto the surface of the second and third plates. This specific binder was chosen to withstand high solar thermal degradation during the hot Algerian summer days.
4. **Integration of the Aluminum Powder:** The pre-weighed aluminum powder was distributed evenly across the adhesive-coated surfaces. For the 20g plate, a lighter micro-roughness layer was formed. For the 40g plate, the particles created a highly dense, packed irregular matrix. The configurations were allowed to cure completely to ensure the particles were permanently anchored to the base metal.
5. **Final Matte Black Coating:** Once cured, all three plates including the smooth reference plate were sprayed uniformly with an identical local matte black-tinted paint. This finalized the optical properties of the surfaces, yielding three distinct structural configurations ready for thermal testing.

Figure II.11: Method of placing filings aluminum

II-6-2 Daily Outdoor Operational Procedure

To collect accurate and reliable thermal data, a rigorous daily protocol was followed during each testing day at the University of El Oued site:

1. **Pre-Test Alignment and Inspection:** Every morning at 07:30, before data collection commenced, the transparent 5 mm glass covers were carefully cleaned with a glass solution to remove any dust or Saharan sand accumulation that could block incoming solar radiation. The structural rack was verified to ensure the collectors remained rigidly fixed at an inclination angle of 33 degrees facing due South.
2. **Sensor and Instrument Calibration:** The thermocouples, pyranometer, and digital handheld meters were checked for proper connectivity and power status to prevent data loss or logging gaps.
3. **Data Logging (08:00 - 16:00):** Starting exactly at 08:00, measurements were recorded simultaneously across all three configurations at fixed 30-minute intervals. At each interval, the parameters logged included: ambient temperature, solar irradiance (W/m^2), inlet air temperature, outlet air temperature, and absorber plate surface temperatures.
4. **Convection Mode Switching:** Testing was carried out over consecutive clear days. On designated passive days, the fluid ports were left completely open to atmosphere to allow pure natural convection (buoyancy-driven flow). On active testing days, the mechanical ventilation fans were engaged at the inlet manifolds, and the digital anemometer was used to adjust and maintain a constant, forced air velocity across the systems.

II-7-1 Assumptions for the Thermal Model

To simplify the complex transient behavior of the fluid flow and heat exchange mechanisms without sacrificing accuracy, the following boundary assumptions were established:

- The solar collector operates under steady-state thermodynamic conditions during each measurement interval.
- Heat flow through the structural wooden casing and the insulation layer is treated as one-dimensional conductive heat transfer.
- The physical and thermal properties of the working fluid (air), such as specific heat capacity and density, are evaluated at the mean fluid temperature.
- Air leakage through the silicone-sealed joints and flow manifolds is assumed to be negligible.

II-7-2 Fundamental Energy Balance Equations

The total solar energy incident on the collector aperture area (A_c) is partly absorbed by the plate and partly lost to the surrounding environment through radiation and convection. The overall energy balance equation for any of the solar collectors can be expressed as:

$$Q_{in} = Q_u + Q_{loss} \tag{1}$$

Where:

- Q_{in} is the total solar energy rate hitting the collector glazing (W).
- Q_u is the useful thermal energy rate collected by the working air stream (W).
- Q_{loss} is the total rate of thermal energy lost to the ambient environment (W).
- The total incident solar power (Q_{in}}) striking the 5 mm glass cover is a function of the clear aperture area (Ac = 0.09 m^2 and the global solar irradiance (It) measured by the pyranometer:

$$Q_{in} = I \cdot A_c \tag{2}$$

II-7-3 Useful Energy Gain (Q_u)

The rate of useful heat energy transferred from the matte black absorber plate configurations to the passing air stream is directly calculated using the temperature rise of the fluid between the inlet and outlet manifolds:

$$Q_u = \dot{m} \cdot C_p \cdot (T_{out} - T_{in}) \tag{3}$$

Where:

- $\dot{m}$ is the mass flow rate of the air working fluid (Kg/s).
- C_p is the specific heat capacity of the air at mean temperature (J/kg.K).
- T_{in} is the temperature of the air entering the inlet manifold (°C).
- T_{out} is the temperature of the air exiting the outlet manifold (°C).

The mass flow rate ($\dot{m}$) is determined by the fluid velocity (V) measured via the digital anemometer, the cross-sectional flow area (A_f), and the temperature-dependent density of air (ρ):

$$\dot{m} = \rho \cdot A_f \cdot V \tag{4}$$

II-7-4 Thermal Efficiency Calculation (η_{th})

The instantaneous thermal efficiency (η_{th}) of each collector configuration is defined as the ratio of the useful thermal energy gained by the air to the total solar energy incident on the aperture area:

$$\eta_{th} = \frac{Q_u}{Q_{in}} = \frac{\dot{m} \cdot C_p \cdot (T_{out} - T_{in})}{I \cdot A_c} \tag{5}$$

By evaluating this equation simultaneously across the smooth reference collector, the 20g aluminum powder collector, and the 40g aluminum powder collector, the direct performance enhancement factor (Δη) achieved by modifying the surface topography can be precisely quantified.

II-7-5 Overall Heat Losses and Fluid Dynamics Metrics

To deeper understand *why* the aluminum powder surfaces perform differently, the total heat loss rate (Q_{loss}) can be broken down using the overall collector heat loss coefficient (U_L), which combines top (glazing), bottom, and edge losses:

$$Q_{loss} = U_L \cdot A_c \cdot (T_{pm} - T_a) \tag{6}$$

Where:

- UL is the overall heat loss coefficient of the collector ($W/m^2.K$).

- T_{pm} is the mean temperature of the absorber plate (°C), calculated as the average of the thermocouple sensors fixed across its surface.
- T_a is the ambient air temperature (°C).

To evaluate the effectiveness of the energy transfer from the plate to the air stream, the collector heat removal factor (F_R) is introduced. It represents the ratio of the actual useful energy gain to the maximum possible energy gain if the entire absorber plate were at the inlet fluid temperature:

$$F_R = \frac{\dot{m} \cdot C_p \cdot (T_{out} - T_{in})}{A_c \cdot [I \cdot (\tau\alpha) - U_L \cdot (T_{in} - T_a)]} \tag{7}$$

Where:

- $\tau\alpha$ is the effective transmittance-absorptance product of the 5 mm glass cover and matte black plate combined.

Finally, to characterize the fluid flow regime under the active forced convection phase, the dimensionless Reynolds number (Re) is determined inside the air duct:

$$Re = \frac{\rho \cdot V \cdot D_h}{\mu} \tag{8}$$

Where:

- V is the average air velocity (m/s) recorded by the digital anemometer.
- D_h is the hydraulic diameter of the collector air flow channel (m).
- μ is the dynamic viscosity of the air fluid (kg/m.s).

By calculating Re, the study can quantitatively show how the 20g and 40g aluminum configurations trigger an early transition from laminar to turbulent flow, increasing the convective heat transfer coefficient.

II-8 Conclusion

This chapter detailed the experimental infrastructure, materials, and mathematical framework developed to evaluate heat transfer enhancement using localized metallic micro-roughness. Three small-scale flat-plate solar air collectors with identical internal dimensions of 30 cm by 30 cm were successfully constructed using cost-effective, locally sourced products. While maintaining uniform parameters across the structural wood frames, 5 mm glass covers, and polystyrene-aluminum insulation layers, the surface profile of the absorber plates was systematically varied. These variations included a smooth control baseline, a 20g aluminum powder matrix, and a 40g aluminum powder matrix.

The complete experimental setup was instrumented with calibrated thermocouples, a pyranometer, and a digital anemometer to continuously log thermodynamic data under real

Saharan meteorological conditions in El Oued, Algeria. Furthermore, the operational procedure was evaluated under both buoyancy-driven natural convection and fan-driven forced convection regimes. The raw data collected through these procedures will be processed using the governing energy balance and fluid dynamics equations established herein. The resulting thermal efficiency curves, temperature gradients, and performance enhancement factors are presented, analyzed, and thoroughly discussed in the following chapter.

III-1 Introduction

This chapter presents the experimental results obtained from three flat-plate solar collector collectors operating under natural and forced convection conditions. The analysis focuses on the effect of absorber surface properties, thermal insulation, airflow configuration, and tilt angle on the thermal performance of the collectors. The evaluation is based on temperature profiles, outlet air temperature, and temperature difference (ΔT), which are used as main indicators of thermal behavior and useful heat gain.

III-2 Methodology

III-2-1 Experimental Procedure

The experimental study was carried out using three flat-plate solar thermal collectors having similar geometrical dimensions and structural characteristics. The only difference between the three collectors was the variation in the absorber surfaces, with the objective of investigating the effect of absorber surface characteristics on the thermal performance of the solar collectors. All collectors were installed at a fixed tilt angle of 33° to ensure optimal solar radiation reception under local climatic conditions. The experiments were conducted under outdoor weather conditions during sunny days using two operating modes: natural convection and forced convection. Measurements were recorded from 08:30 a.m. to 14:00 p.m. under direct solar radiation conditions, followed by an additional measurement period from 14:30 p.m. to 15:00 p.m. under shaded conditions in order to study the thermal behavior of the collectors after the decrease in solar radiation intensity. Several thermal and meteorological measuring instruments were used during the experiments. Thermocouples were employed to measure temperatures at different locations inside the solar collector, including the absorber surface temperature, the inner and outer glass temperatures, the chamber temperature inside the collector, and the outlet fluid temperature. An anemometer was used to measure the outlet fluid flow velocity under both natural and forced convection conditions, while a pyrometer was used to measure the solar radiation intensity incident on the collector surface throughout the experimental period. In addition, the ambient temperature was recorded to evaluate the influence of climatic conditions on the thermal performance of the solar collectors. After collecting the experimental data, the results, were analyzed and compared for the three collectors under natural and forced convection conditions in order to evaluate the effect of absorber surface variation and heat transfer mode on the thermal efficiency, and overall performance of the solar collectors.

III-3 Result

III-3-1 Forced Convection

III-3-1-1 Solar Radiation and Ambient Temperature of Forced convection

The environmental conditions recorded during the experimental testing period from 08:30 to 15:00 are illustrated across the profiles as shown in Figure III.1. The solar radiation begins at approximately715 Watts per meter squared at 08:30 and rapidly climbs to an early morning peak of nearly 880 Watts per meter squared at 09:00. Following this peak, the solar intensity undergoes a gradual, continuous decline throughout the midday period, dropping sharply after 14:00 to fall below 100 Watts per meter squared by 15:00. In contrast to the solar intensity curve, the ambient temperature exhibits a steady, progressive increase as the day advances. Starting from a morning baseline of 23°C at 08:30, the ambient air temperature warms up gradually to reach its maximum peak of approximately 34°C at around 14:00, before beginning a mild decline toward the end of the test.

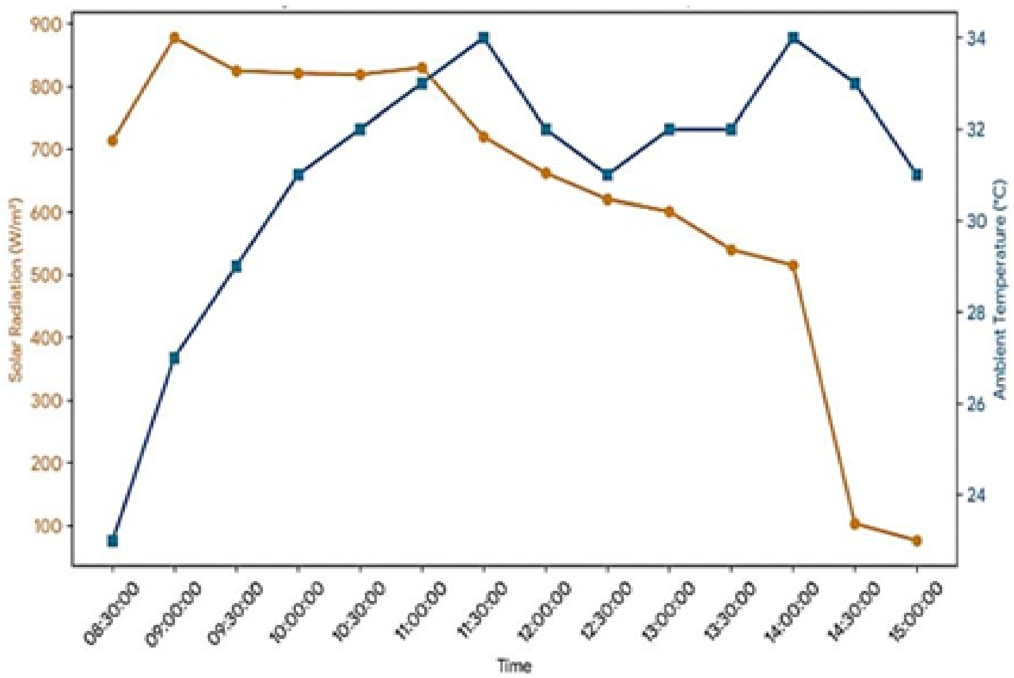

Figure III.1: Solar radiation and ambient temperature forced

III-3-1-1-2 External Glass Cover Temperature (T_{ext})

The thermal response of the outer protective layer as shown in Figure III.2. The external glass surface temperatures, represented by $T_{G.ex1}$, $T_{G.ex2}$, and $T_{G.ex3}$, rise steadily from an initial value near 25 °C at 08:30 to peak values between 54 °C and 56 °C around 12:00. A noticeable secondary thermal peak occurs around 14:00, with temperatures reaching approximately 51 °C to 53 °C. Structural thermal inertia and the high ambient air, temperature at that hour, drive a secondary peak after which the values drop rapidly through the late afternoon to reach a minimum by 15:00.

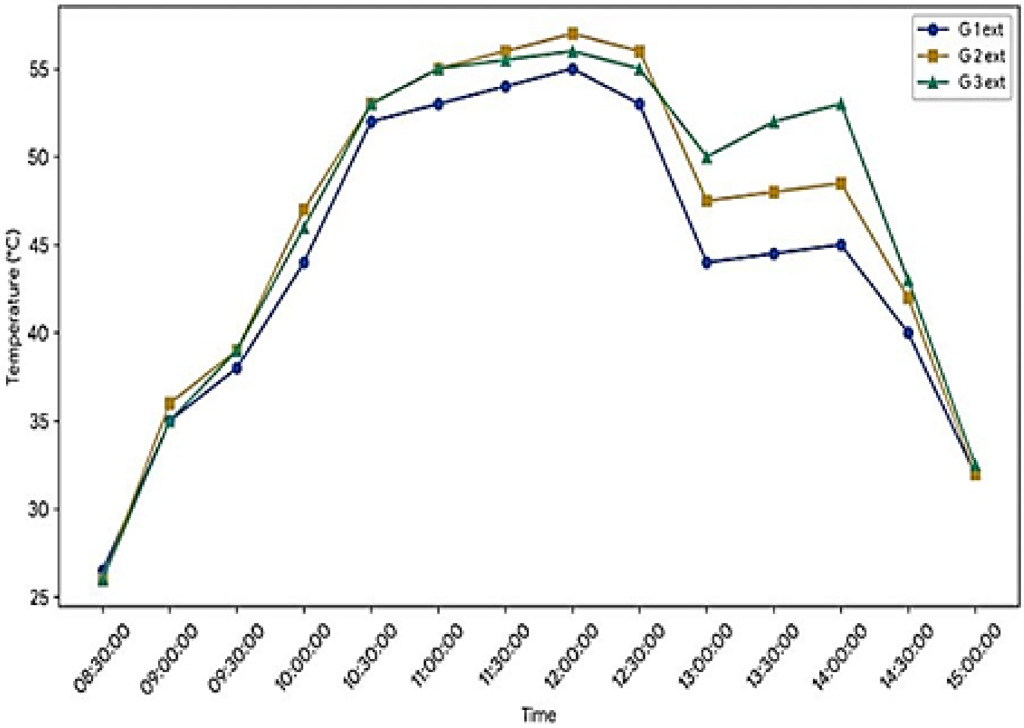

Figure III.2: Diurnal variations of external glass cover temperatures

III-3-1-1-3 Internal Glass Cover Temperature (T_{int})

The internal glass cover temperatures $T_{G.int1}$, $T_{G.int2}$, $T_{G.int3}$ are presented in Figure III.3. Due to the greenhouse effect trapped within the collector structure, the inner surface of the glazing achieves significantly higher thermal thresholds than the external surface. Starting at roughly 28°C to 30°C at 08:30, the internal temperatures surpass 60°C by 10:30. Unlike the solar radiation curve, which falls continuously after its early morning peak, the internal glass temperatures continue to climb due to heat accumulation, reaching their maximum values between 65°C and 69°C at 14:00. This clear thermal lag demonstrates effective energy containment within the collector casing, where $Tint_3$ consistently exhibits the highest thermal performance among the three measured points.

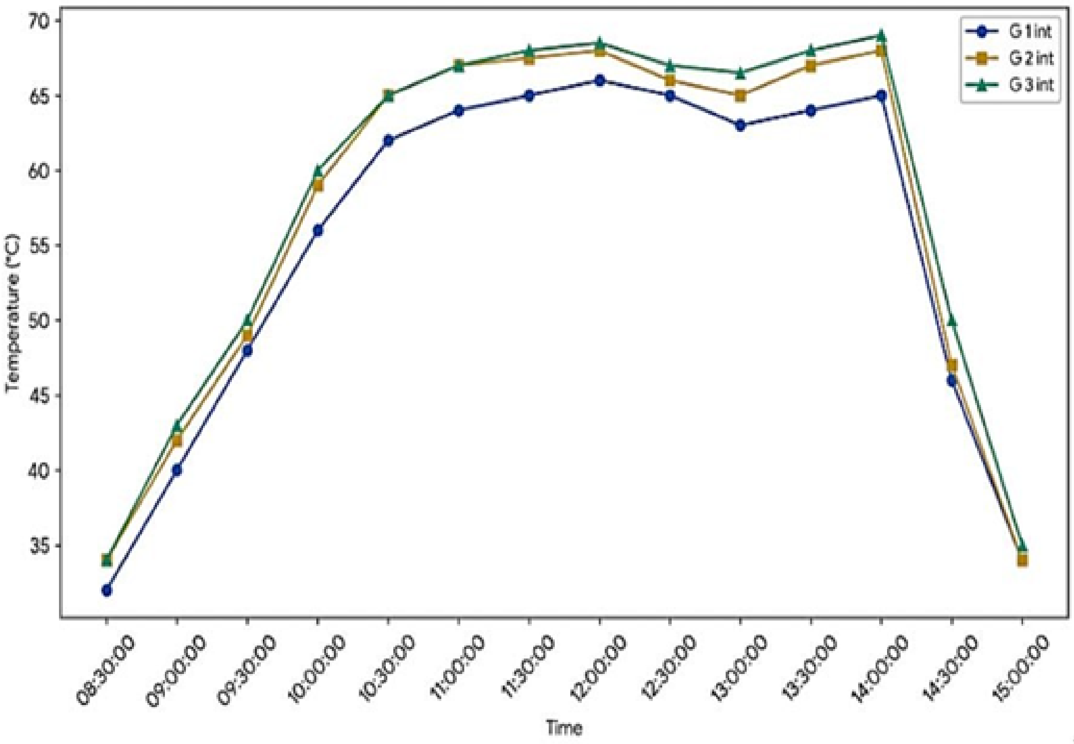

Figure III.3: Transient response of internal glass cover profiles

III-3-1-1-4 Room Temperature (T room)

The temperature profiles recorded within the internal cavity or room (T room) of the solar collector setup as shown in Figure III.4. The air cavity temperatures rise sharply during the morning hours, accelerating from an average of 26°C at 08:30 to breach the 70°C mark by 10:00. Throughout the mid-day period (10:00 to 12:30), the cavity stabilizes into a thermal plateau hovering around 72°C to 77°C. Driven by prolonged thermal absorption, the peak cavity temperatures are captured at 14:00, where T room3 reaches a maximum of 84°C, followed closely by T room2 (82°C) and T room1 (79°C). The substantial gap maintained between T room and the ambient temperature curve (which maxes out at 34°C) demonstrates high structural heat retention capacity.

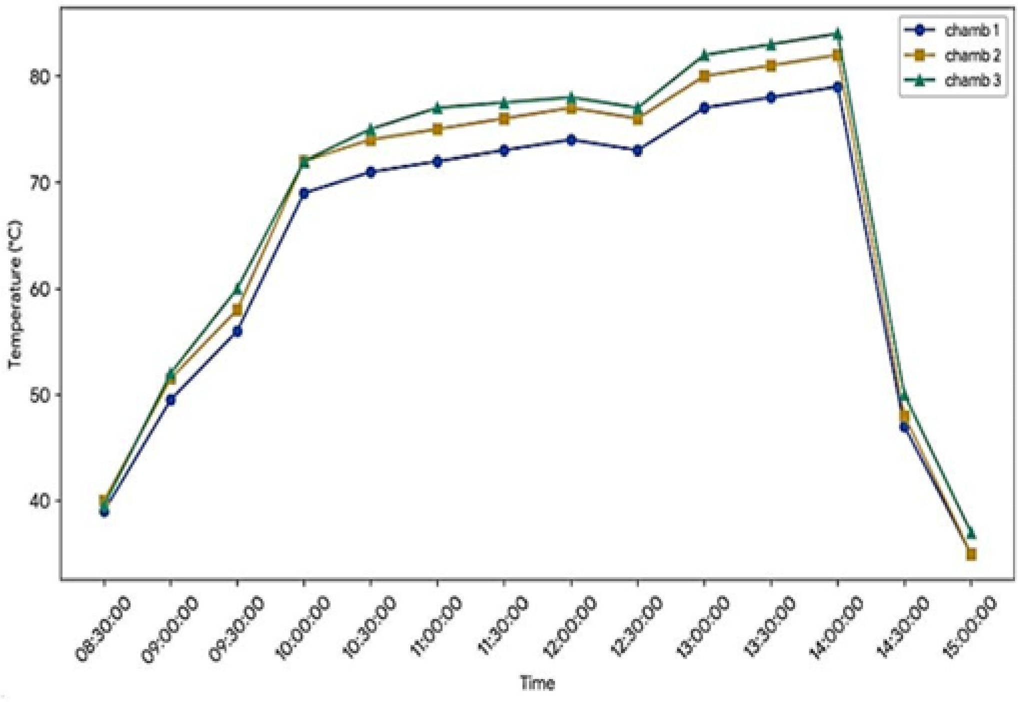

Figure III.4: Dynamic evaluation of the collector inner room/air cavity temperatures

III-3-1-1-5 Absorber Plate Temperature (T_{abs})

The thermal evolution of the primary solar absorber plate elements (T_{abs1}, T_{abs2}, T_{abs3}) is detailed in Figure III.5. As the engine of the thermal collector, the absorber plate records the highest temperatures within the entire system. From an initial state of 40°C at 08:30, the absorber plate heats rapidly, reaching a high- temperature plateau above 75°C as early as 10:30. Due to the high heat capacity of the absorber material and sustained infrared trapping, the curves peak at 14:00. At this peak, T abs3 attains a maximum value of approximately 91°C, while T abs2 and T abs1 reach 88°C and 86°C, respectively. The sharp drop in absorber temperatures after 14:00 mirrors the rapid loss of direct solar input, confirming the direct dependency of the plate's thermal state on incident solar flux.

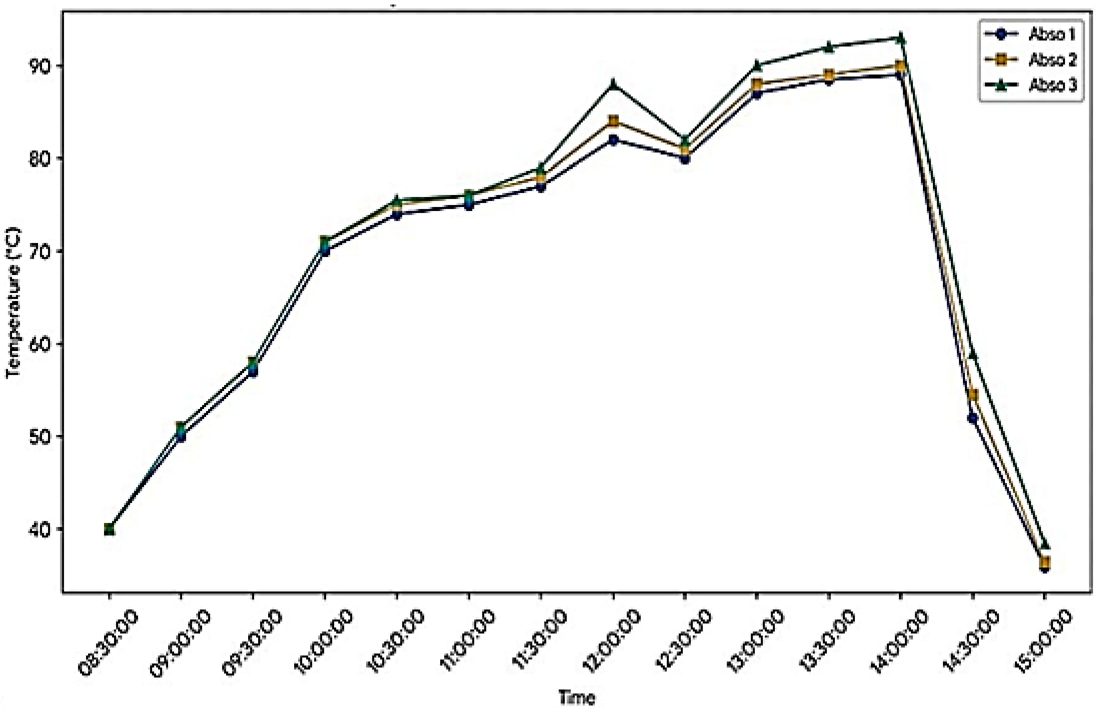

Figure III.5: Thermal behavior of the collector absorber plates

III-3-1-1-6 Fluid Outlet Temperature Analysis

As shown in Figure III.6, the fluid outlet temperatures, represented by T_{Out1}, T_{Out2}, and T_{Out3}, rise steadily from an initial value near 40 °C at 08:30 to breach the 60 °C threshold by 10:00. This rapid morning heating indicates a strong thermal response to the high early solar irradiance. The Figure III.6 represents an interesting trend between 10:00 and 14:00, where the outlet temperatures continue to climb progressively despite the steady decline in solar radiation. This behavior is due to thermal lag, meaning the collector effectively stores heat within its structure and continuously transfers it to the working fluid. The maximum fluid temperatures are recorded at 14:00, where T Out3 reaches the highest value at approximately 76 °C, followed closely by T_{Out2} at 75 °C and T Out1 at 73 °C. After 14:00, the temperatures drop sharply, directly mirroring the collapse of solar radiation. By the end of the test at 15:00, the fluid outlet temperatures decline to a range between 35 °C and 37 °C. The close agreement among the three curves confirms uniform fluid distribution and stable heat gain throughout the system

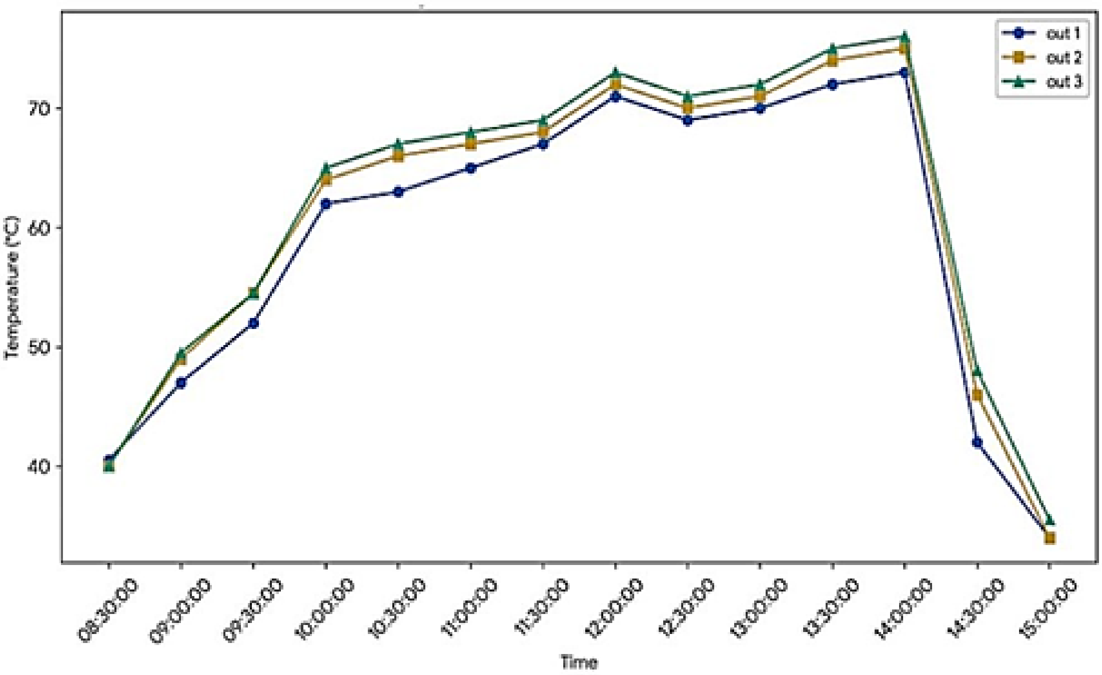

Figure III.6: Transient variation of fluid outlet temperatures

III-3-1-1-7 Outlet Flow Rate Behavior of the Three Collector Configurations

As shown in the Figure III.7, the outlet flow rates of the three collectors ($Flow._{Out\ 1}$, $Flow._{Out\ 2}$, and $Flow._{Out\ 3}$) exhibit varying behavior throughout the experimental testing period from 08:30 to 15:00. All flow rates start at zero (0.000) at 08:30 and then increase suddenly and equally to 0.100 at 09:00, indicating the start of the fluid circulation system. At 10:00, differences in performance begin to appear, as the outlet flow rates of Collectors 1 and 3 increase to 0.200, while Collector 2 remains at 0.100. At 11:00, the flow rate of Collector 1 decreases to 0.100, whereas Collectors 2 and 3 increase to 0.200. At 11:30, Collector 3 remains at 0.200 while Collectors 1 and 2 decrease to 0.100. By 12:00, all three collectors reach the same flow rate value of 0.100. At 12:30, all collectors maintain a stable flow rate of 0.100. At 13:00, Collector 3 records the highest flow rate of the experiment, reaching 0.200, while Collectors 1 and 2 remain at 0.100. At 13:30, all three collectors return to 0.100, and this condition continues until 14:00. Finally, at 15:00, all outlet flow rates decrease to zero (0.000), marking the end of the operating period. The variations observed in the outlet flow rates indicate that the three collectors were subjected to different operating conditions during certain periods of the experiment. Despite these fluctuations, the flow rates remained within a limited range of 0.100–0.200, ensuring continuous fluid circulation throughout the test. The higher flow rate recorded by Collector

3 at 13:00 may have contributed to enhanced heat transfer and improved thermal performance compared with the other collectors. Overall, the flow rate profiles confirm stable system operation and provide a reliable basis for comparing the thermal behavior of the three collector configurations.

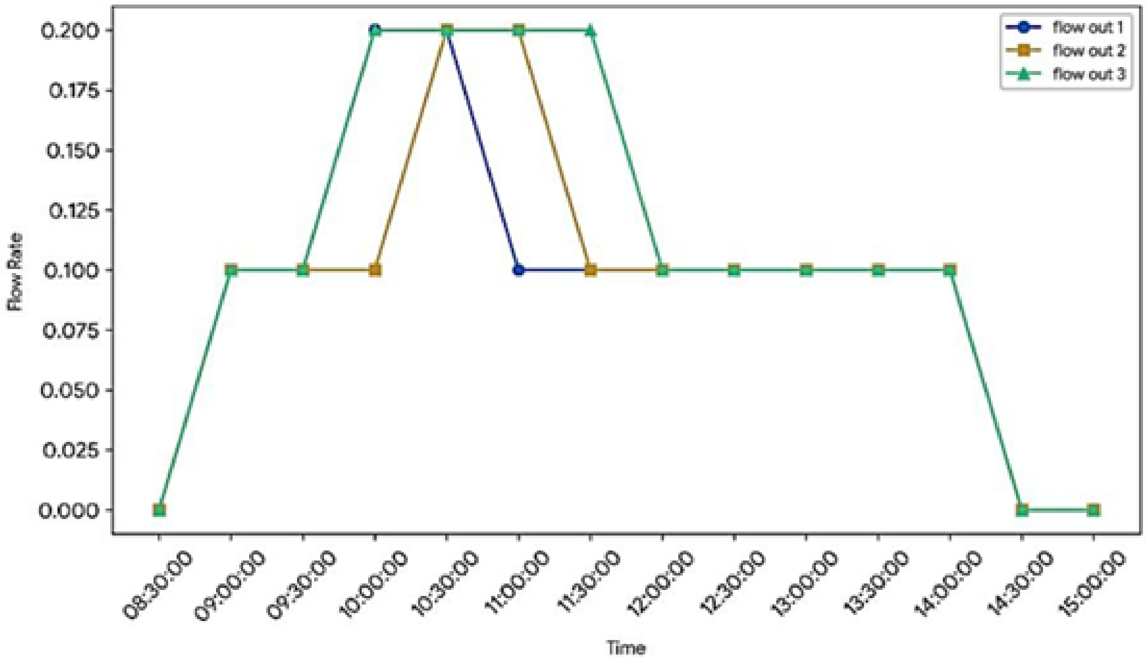

Figure III.7: Outlet Flow Rate Profiles

III-3-1-8 Performance under Forced Convection

The thermal efficiency behavior under a pump-driven forced convection configuration is presented in Figure III.8. Unlike the natural convection mode, the forced convection arrangement forces an immediate and steady fluid circulation across the channels right from the start of the daily cycle. Consequently, all three collectors initiate useful heat removal and record measurable thermal efficiency values as early as 09:00, with initial efficiencies hovering between 10.59% and 11.91%. By forcing a constant fluid velocity, the convective heat transfer coefficient (h) inside the tubes is significantly amplified, permitting rapid thermal extraction from the absorber plates during the peak radiation window.

The relative performance rank among the collectors remains consistent with the previous configuration, proving the robust impact of the material modification. Collector 3 (40 g Al powder) maintains its dominant position, operating at an efficiency advantage over

Collector 2 (20 g Al powder) and the Reference Collector (Collector 1) throughout the afternoon. While the reference collector reaches a plateau around 35.21%, the insertion of 40 g of powder aluminum enables Collector 3 to achieve an elevated and sustained thermal efficiency peak of approximately 37.91%. The smoothing of the curve indicates that forced convection dampens sudden environmental fluctuations, resulting in a more stable and predictable heat extraction rate.

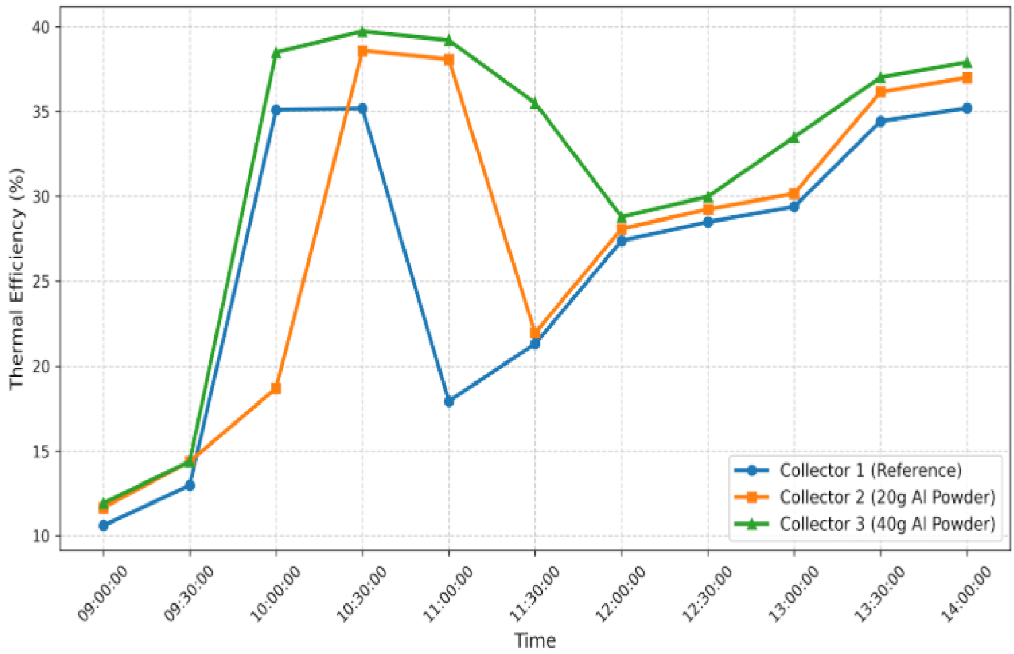

Figure III.8: Performance under Forced Convection

III-3-2 Natural Convection

III-3-2-1 Solar Radiation and Ambient Temperature of Natural Convection

The environmental conditions recorded during the experimental testing period from 08:30 to 15:00 are illustrated as shown in Figure III.9. The solar radiation starts at approximately 700 W/m² at 08:30 and increases rapidly during the early morning hours, reaching a maximum value close to 880 W/m² between 09:00 and 09:30. After this initial peak, the solar intensity shows slight fluctuations around 820–840 W/m² until nearly midday. Beyond 12:00, the radiation begins a continuous gradual decrease, dropping to nearly 520 W/m² at 14:00 before experiencing a sharp decline after 14:30, finally reaching values below 100 W/m² by 15:00. In contrast, the ambient temperature follows a progressively increasing trend throughout the day. Starting from approximately 22°C at 08:30, the temperature rises steadily as solar exposure continues, reaching around 33–34°C during the afternoon period. A slight temporary reduction is observed near 12:30; however, the ambient temperature quickly recovers and attains its highest value at approximately 14:00. Toward the end of the experiment, the temperature decreases moderately as the solar radiation intensity significantly weakens.

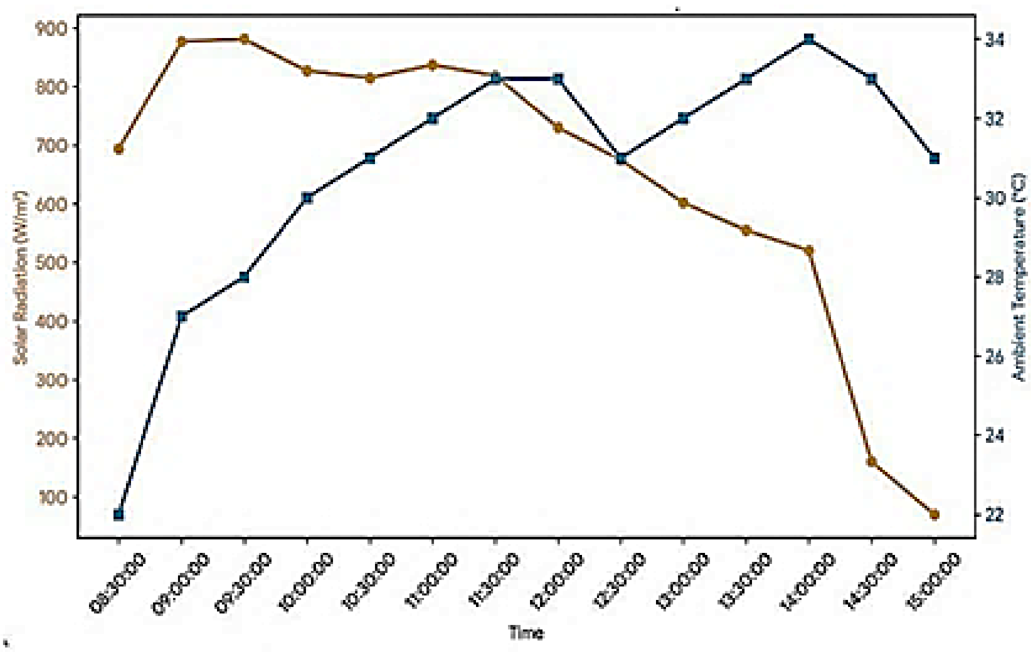

Figure III.9: Solar radiation and ambient temperature natural

III-3-2-2 Absorber Plate Temperature (T abs)

The absorber temperature profiles of the three collectors recorded during the experimental testing period from 08:30 to 15:00 are illustrated in Figure III.10. The absorber temperatures of all collectors begin at approximately 37–38°C at 08:30 and increase rapidly during the morning period as solar exposure intensifies. By 09:00, the temperatures rise to nearly 50°C, continuing their progressive increase throughout the day. Around 10:30, the absorber temperatures exceed 70°C for all configurations, indicating significant heat absorption within the collectors. Among the three curves, Collector 3 (T_{Abs3}) consistently exhibits the highest thermal response during almost the entire testing period. Its temperature reaches approximately 87°C at 12:00 and continues increasing to attain a maximum peak close to 94°C at around 14:00. Collector 2 (T_{Abs2}) follows a similar trend with slightly lower values, while Collector 1 (T_{Abs1}) records the lowest absorber temperatures throughout the experiment. A slight temperature reduction is observed around

12:30 for the three collectors, after which the temperatures recover and continue increasing progressively during the afternoon period. Following the maximum peak at nearly 14:00, all absorber temperatures undergo a sharp and sudden decline, dropping significantly after 14:30 and reaching values close to 36–39°C by 15:00. This rapid decrease is mainly, attributed to the strong reduction in solar radiation intensity near the end of the experimental test.

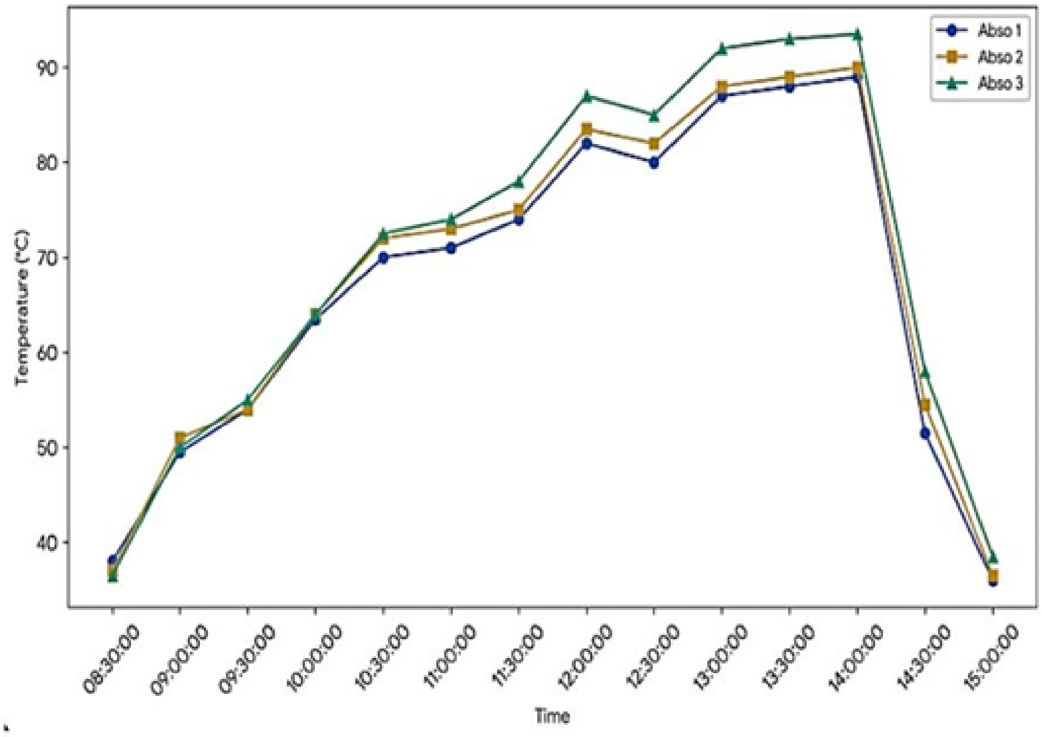

Figure III.10: Thermal behavior of the collector absorber plates

III-3-2-3 Fluid Outlet Temperature Analysis

The outlet air temperature, profiles of the three collectors recorded during the experimental testing period from 08:30 to 15:00 are illustrated in Figure III.11. The outlet temperatures of all collectors begin at approximately 36–37°C at 08:30 and increase steadily during the morning hours as solar heating intensifies. By 09:00, the outlet temperatures reach around 41°C, 45°C, and 46°C for Collector 1, Collector 2, and Collector 3, respectively. A rapid rise is then observed between 09:30 and 10:30, where the temperatures exceed 60°C and continue to increase progressively throughout the day. During the midday period, the outlet temperatures remain relatively stable, fluctuating between 68°C and 78°C. The highest temperatures are recorded around 14:00, reaching approximately 73°C for Collector 1, 76°C for Collector 2, and 78°C for Collector 3. Throughout the testing period, Collector 3 consistently exhibits the highest outlet temperature, followed by Collector 2, while Collector 1 records the lowest values. After 14:00, a sharp decrease in outlet temperature is observed for all collectors, corresponding to the significant reduction in solar radiation. By 15:00, the outlet temperatures drop to nearly 34–36°C, approaching their initial morning values.

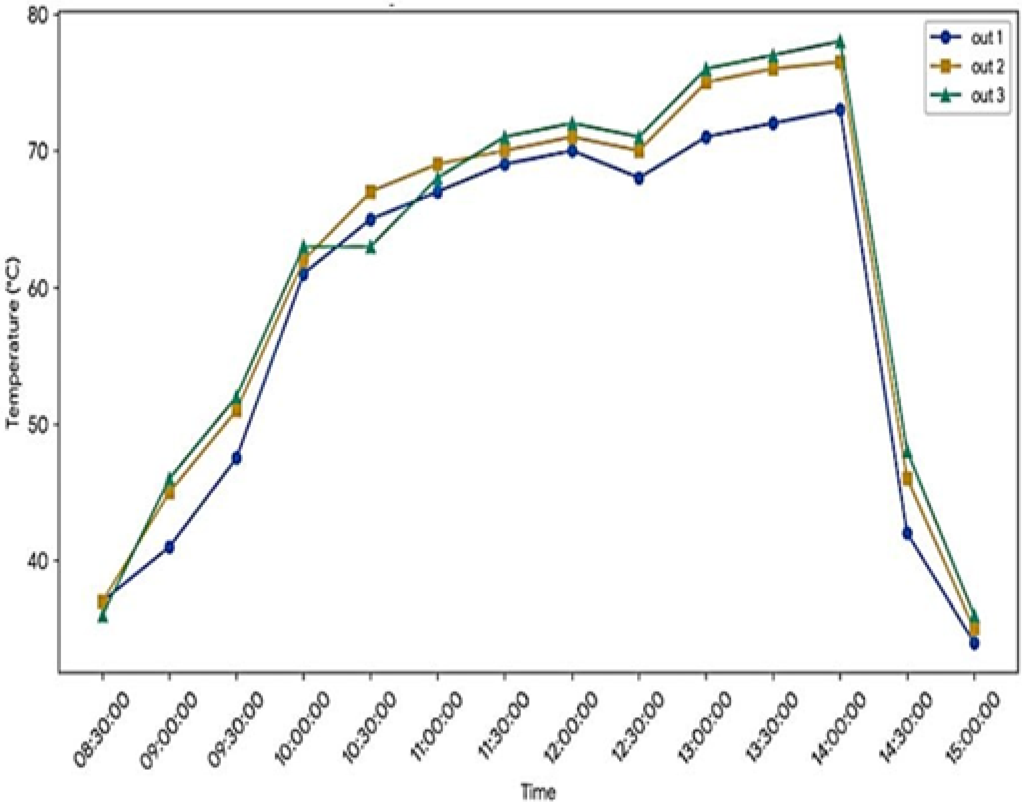

Figure III.11: Fluid Outlet Temperature Analysis

III-3-2-4 External Glass Temperature Profiles

As shown in Figure III.12, the external glass temperatures represented by T_{G1ext}, T_{G2ext}, and T_{G3ext} exhibit a similar thermal behavior throughout the experimental period. The temperatures begin at approximately 26–27 °C at 08:30 and increase rapidly during the morning hours due to the increasing solar exposure. By 10:30, all three collectors experience a sharp rise, reaching temperatures above 50 °C, indicating significant heat absorption by the collector glazing. The temperatures continue to increase gradually, reaching their peak values around midday. Collector 3 records the highest external glass temperature of approximately 56 °C at 12:00–12:30, followed closely by Collector 2 at 55 °C, while Collector 1 reaches about 54 °C. After midday, a noticeable decrease occurs, with temperatures dropping to approximately 44–46 °C at 13:00. A slight recovery is observed between 13:30 and 14:00 before all temperatures decline sharply toward the end of the test period. At 15:00, the external glass temperatures fall to nearly 32–33 °C. The consistently higher temperatures recorded by Collector 3 indicate enhanced heat retention and solar energy absorption, while the small temperature differences among the three curves demonstrate comparable glazing performance under the same environmental conditions.

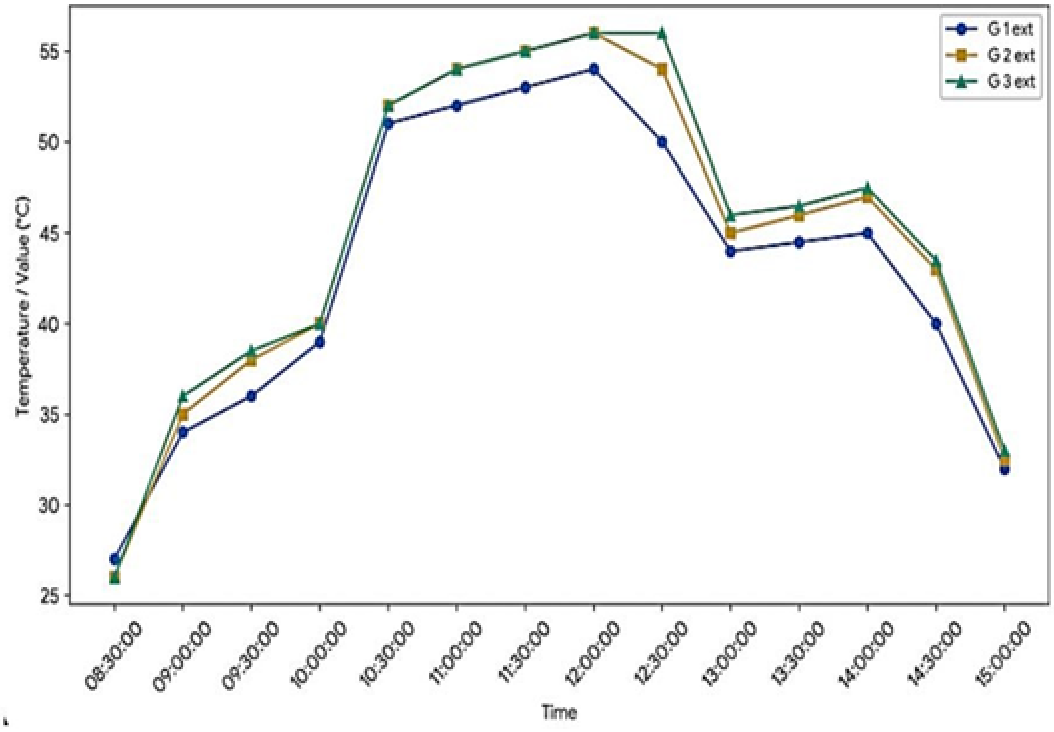

Figure III.12: Fluid Flow Rate Variation during the Experimental Period

III-3-2-5 Internal Collector Temperature Profiles

As shown in Figure III.13, the internal collector temperatures (T_{G1int}, T_{G2int}, and T_{G3int}) increase progressively throughout the experimental period as solar energy is absorbed and stored within the collector system. At 08:30, the temperatures start at approximately 31.5 °C, 32.5 °C, and 32 °C for G1int, G2int, and G3int, respectively. During the morning period, all temperatures rise rapidly due to the increase in solar irradiance, exceeding 50 °C before midday. Between 10:00 and 14:00, the temperature profiles continue to increase despite the gradual decline in solar radiation, demonstrating the thermal inertia of the collector and its ability to retain and transfer heat efficiently. The highest temperatures are recorded at approximately 14:00, with G3int reaching a maximum value of about 71 °C, followed by G2int at 64 °C and G1int at 59 °C. The significantly higher temperature achieved by G3int indicates enhanced thermal performance and greater heat retention capability compared with the other configurations. After 14:00, all temperatures decrease rapidly as solar irradiance diminishes and thermal losses become dominant. By 15:00, G1int and G2int fall to approximately 34 °C, while G3int remains slightly higher at about 35 °C. Overall, the results demonstrate effective heat absorption and stable thermal behavior for all collectors, with Collector 3 exhibiting the best thermal performance throughout the experimental period.

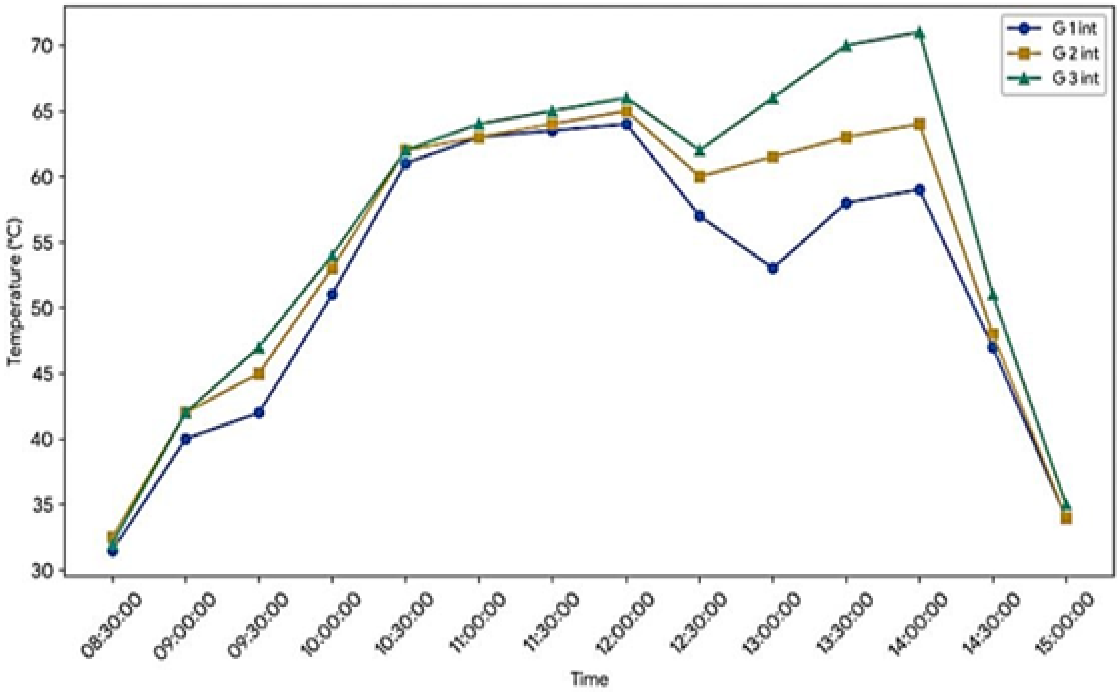

Figure III.13: Variation of Internal Collector Temperatures during the Experimental Period

III-3-2-6 Chamber Temperature Profiles

As shown in Figure III.14, the chamber temperatures represented by T_{Chamb1}, T_{Chamb2}, and T_{Chamb3} increase steadily throughout the morning period as solar energy is absorbed and accumulated within the collector systems. Starting from approximately 38 °C at 08:30, the temperatures rise rapidly and exceed 60 °C by 10:00. A further increase is observed between 10:30 and 12:00, where chamber temperatures reach values between 73 °C and 78 °C. The highest temperatures are recorded during the early afternoon period, with T_{Chamb3} achieving the maximum value of approximately 79 °C at 14:00, followed by T_{Chamb2} at nearly 78 °C, while T_{Chamb1} reaches about 74 °C. Despite minor fluctuations around midday, the chamber temperatures remain relatively high, reflecting the strong thermal storage capacity of the collector structure and the continuous accumulation of solar heat. Following 14:00, all curves exhibit a sharp decline as solar input decreases and heat losses become dominant. By 15:00, the chamber temperatures fall to approximately 35–37 °C. The consistently higher temperatures obtained by Collector 3 suggest superior thermal insulation and heat retention characteristics, whereas the close agreement among the three curves indicates stable and repeatable thermal behavior across the tested collectors.

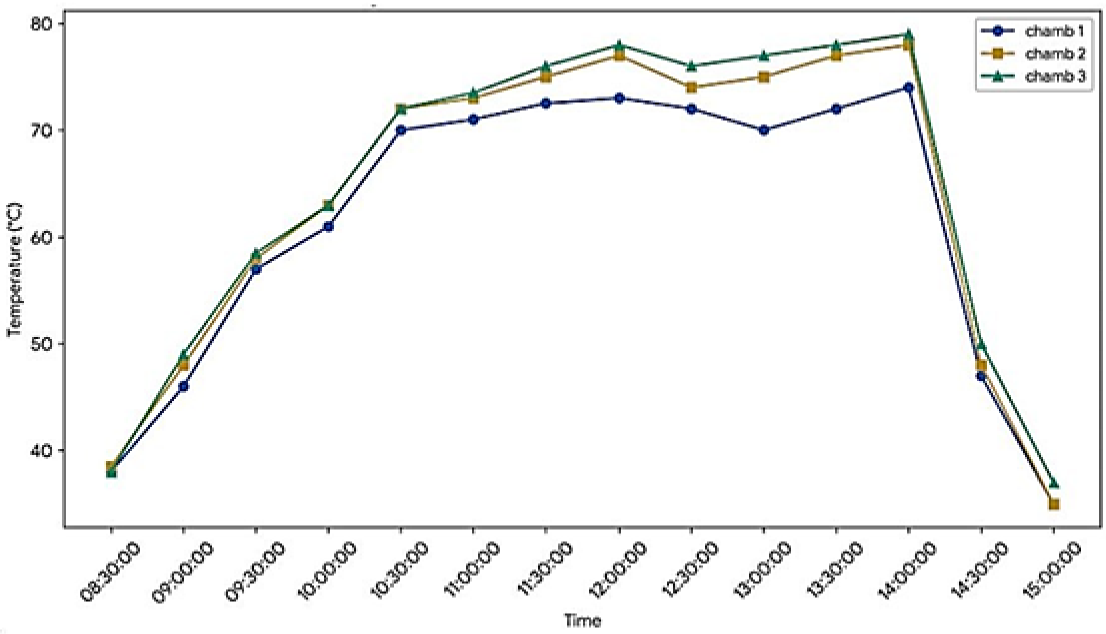

Figure III.14: Comparison of Chamber Temperatures of the Three Collectors

III-3-2-7 Fluid Flow Rate Variation during the Experimental Period

As shown in Figure III.15, the flow rate profiles of the three collectors, represented by Flow $_{Out1}$, Flow $_{Out2}$, and Flow $_{Out3}$, illustrate the operating conditions of the forced-convection experiment. During the initial period from 08:30 to approximately 10:00, the flow rates remain at zero, indicating that no forced circulation is applied and the system operates under natural conditions. At 10:00, the flow rates of Collectors 1 and 3 increase abruptly to 0.1, while Collector 2 reaches the same value slightly later at approximately 10:30. From this point until 14:00, all three collectors maintain a constant flow rate of 0.1, demonstrating stable fluid circulation throughout the active testing period. Such a constant flow rate ensures that differences in thermal performance are primarily related to collector design rather than variations in fluid movement. At approximately 14:30, the circulation is stopped and the flow rates immediately return to zero for all collectors, remaining at this level until the end of the experiment. The identical flow-rate profiles confirm uniform operating conditions and provide a reliable basis for comparing the thermal behavior of the three collector configurations.

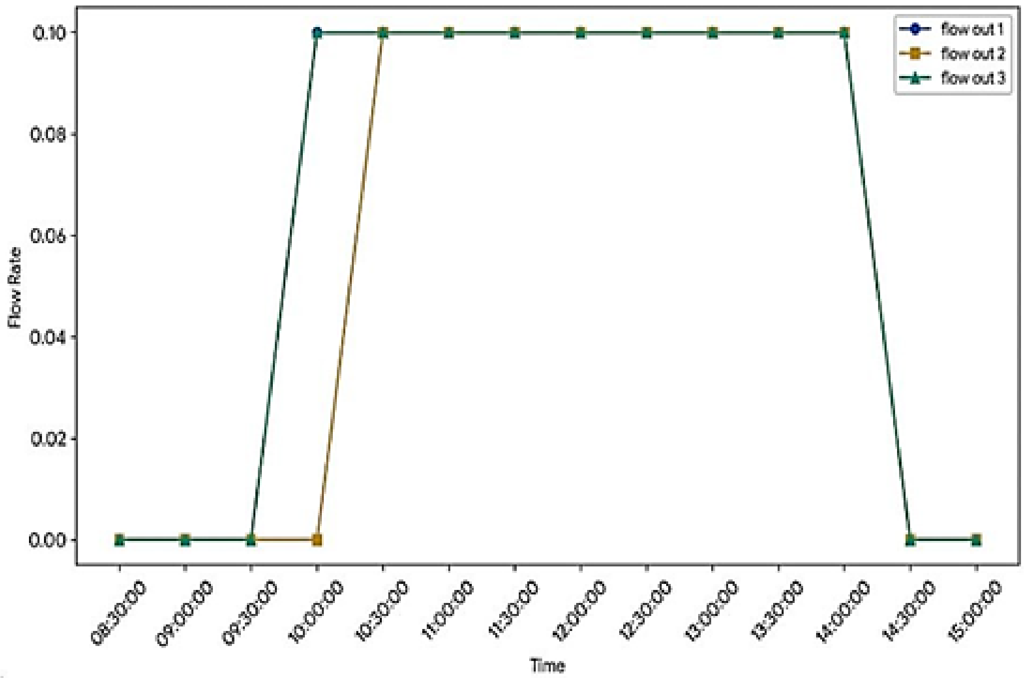

Figure III.15: Fluid Flow Rate Variation during the Experimental Period

III-3-2-8 Performance Under Natural Convection

Figure III.16, illustrates the diurnal variation of the hourly thermal efficiency (η) for the three tested solar collectors operating under natural convection mode. It can be clearly observed that the thermal efficiency profiles follow a progressive parabolic trend that closely mirrors the ambient solar irradiance cycle. During the early morning hours (08:30 to 09:30), the thermal efficiency remains at zero for all systems because the thermosyphon driving head has not yet overcome the fluid's internal friction and flow resistance. Active thermal gain begins at 10:00, after which the efficiency curves climb steadily to reach their peak values at approximately 14:00.

The experimental data clearly highlights the significant impact of the powder aluminum (Al) coating on the absorber plates. Collector 3 (coated with 40 g of powder Al) consistently records the highest thermal efficiency throughout the day, achieving a maximum peak efficiency of approximately 39.34%. This is followed by Collector 2 (coated with 20 g of powder Al), which reaches a peak of 38.00%. In contrast, Collector 1 (the Reference system) exhibits the lowest performance, maxing out at 34.87%. This noticeable enhancement is directly attributed to the superior thermal conductivity of the powder aluminum (k = 205 W/m.K), which minimizes localized thermal resistance across the absorber plate. Furthermore, the micro-powder layer increases the contact surface area between the absorber and the fluid channels, maximizing the useful heat gain (Q_{useful}) transferred to the water and demonstrating that increasing the mass from 20 g to 40g yields a progressive thermal Benefit.

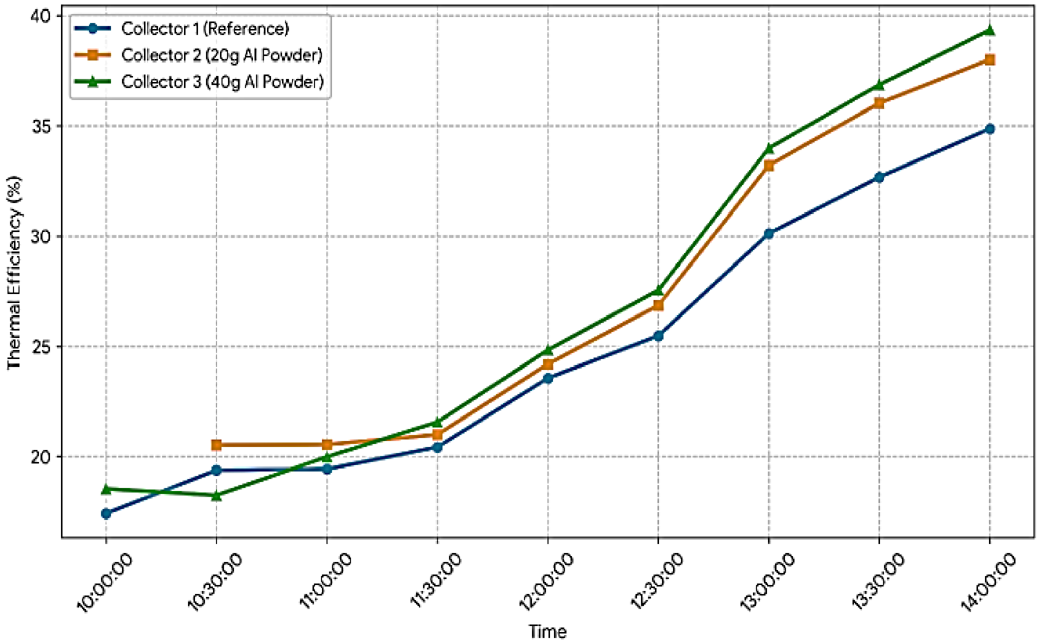

Figure III.16: Performance Under Natural Convection

III-3-3 Thermal Efficiency Calculation

-The thermal efficiency (η) of a flat-plate liquid solar collector is defined as the ratio of the useful heat power gained by the working fluid (Q̧ useful) to the total solar radiation energy incident upon the collector's aperture area (Q̧ solar).

$$\eta = \frac{\dot{Q}_{useful}}{\dot{Q}_{solar}}$$

Expanding this into operational variables yields the standard engineering equation used to evaluate your experimental data:

$$\eta = \frac{\dot{m} \, . \, C_p \, . \, (T_{out} - T_{in})}{G \, . \, A_c}$$

Where:

η: Thermal efficiency of the collector (expressed as a fraction or percentage).

$\dot{m}$: Mass flow rate of the working fluid .

C_p: Specific heat capacity of the fluid. For water, this constant is taken as approximately 4184 J/kg.K).

T_{out}: Outlet fluid temperature, corresponding to your measured columns out 1, out 2, and out 3.

T_{in}: Inlet fluid temperature. Since your experimental configuration did not utilize a separate preheating loop, it is physically established that the fluid enters at the surrounding temperature, meaning:

$$T_{in} = T_{amb}$$

G: Total global solar radiation incident on the collector surface (W/m'), corresponding to your column solar radiation.

A_c: Clear aperture area of a single solar collector (m').

III-4 Comparison of the Thermal Performance of the Three Solar Collector Collectors

The comparison presented in Table III.1 clearly demonstrates that Collector 3 achieved the best overall thermal performance among the three tested configurations under both natural and forced convection conditions. It consistently recorded the highest temperatures and thermal showed intermediate performance, while Collector 1 exhibited the lowest thermal response. These results confirm the positive effect of powder aluminum addition on the absorber surface, as increasing the powder aluminum content improved heat transfer and enhanced the overall efficiency of the solar collector. Therefore, Collector 3 can be considered the most effective configuration for maximizing the thermal performance of the flat-plate solar collect

Table III.1: Comparison of Peak Thermal Performance Parameters for the Three Collectors under Natural and Forced Convection

Parameter	Collector 1	Collector 2	Collector 3
Absorber Temperature, Forced Convection ($T_{abs,max}$)	89C°	90C°	93C°
Absorber Temperature, Natural Convection ($T_{abs,max}$)	89C°	90C°	93,5C°
Outlet Fluid Temperature, Forced Convection ($T_{out,max}$)	0,2	0,2	0,2
Outlet Fluid Temperature, Natural Convection ($T_{out,max}$)	0,1	0,1	0,1
External Glass Temperature Forced convection ($T_{Gext,max}$)	55C°	57C°	56C°
External Glass Temperature Natural convection ($T_{Gext,max}$)	55C°	57C°	56C°
Internal Glass Temperature Forced convection ($T_{Gint,max}$)	66C°	68C°	69C°
Internal Glass Temperature Natural convection ($T_{Gint,max}$)	64C°	65C°	71C°
Chamber Temperature Forced Convection ($T_{Chamb,max}$)	79C°	82C°	84C°
Chamber Temperature Natural Convection ($T_{Chamb,max}$)	73C°	78C°	79C°
Thermal Efficiency, Forced Convection	34,21%	=36-37%	37,91%
Thermal Efficiency, Natural Convection	34,87%	38,00%	39,34%
Overall Performance Ranking	3rd	2nd	1st

III-5 Conclusion

This chapter presented and discussed the experimental results obtained from the three flat-plate solar collector collectors operating under both natural and forced convection conditions at a tilt angle of 33°. The analysis was based on the variation of solar radiation, ambient temperature, absorber temperature, glass cover temperatures, chamber temperature, outlet fluid temperature, flow rate, and thermal efficiency. The results demonstrated that all collectors responded effectively to solar radiation throughout the testing period, with temperatures increasing progressively during the day and reaching their maximum values around 14:00. The thermal behavior of the collectors revealed a significant heat storage capacity, as several temperature profiles continued to increase despite the gradual decline in solar irradiance, indicating the presence of thermal inertia within the collector structure. A comparison of the three collectors showed that Collector 3 consistently achieved the highest temperatures and thermal efficiency under both natural and forced convection modes. The absorber temperature reached approximately 91 °C, while the outlet fluid temperature attained about 78 °C under natural convection and 76 °C under forced convection. In addition, Collector 3 recorded the highest chamber and internal glass temperatures, confirming its superior heat absorption and retention capabilities. Collector 2 exhibited intermediate performance, whereas Collector 1 showed the lowest thermal response and efficiency values. The thermal efficiency analysis further confirmed the positive effect of powder aluminum addition on collector performance. The maximum efficiency increased from 34.87% for the reference collector to 39.34% for the collector coated with 40 g of powder aluminum under natural convection conditions. Similar improvements were observed under forced convection operation, where Collector 3 achieved the highest efficiency of approximately 37.91%. Overall, the experimental investigation demonstrates that enhancing the absorber surface with powder aluminum significantly improves heat transfer, thermal storage, and collector efficiency. Among the tested configurations, Collector 3 provided the best overall thermal performance, making it the most promising design for improving the efficiency of flat-plate solar collectors.

General Conclusion

This Master's thesis successfully investigated the design modification and experimental thermal performance of flat-plate solar collectors by incorporating industrial aluminum shavings onto the absorber surface. By testing three custom-fabricated collectors—a standard Reference Collector (Collector 1), a collector with 20 grams of aluminum (Collector 2), and a collector with 40 grams of aluminum (Collector 3)—under real climatic conditions, a clear relationship between passive surface texturing and heat transfer optimization was established.

Core Findings and Experimental Data

- **Thermal Efficiency Gains:** Passive surface modification using aluminum powder proved highly effective. Under natural convection, the maximum thermal efficiency increased from 34.87% for the reference collector to 38.00% for Collector 2, and reached a peak of 39.34% for Collector 3. Under forced convection, Collector 3 achieved the highest efficiency of 37.91% compared to 34.21% for the reference.
- **Absorber Temperature Response:** The modified surfaces recorded significantly higher thermal responses. Under natural convection, the peak absorber temperature reached 93.5°C for Collector 3 and 90°C for Collector 2, while the reference collector maxed out at 89°C. Under forced convection, Collector 3 reached a peak of 93°C.
- **Internal Casing and Insulation Performance:** The structural heat retention capacity was highly apparent in the internal chamber readings. Under natural convection, the peak chamber temperature reached 79°C for Collector 3 and 78°C for Collector 2, leaving the reference collector at 74°C. The peak internal glass temperature also showed enhanced trapping, hitting 71°C for Collector 3 compared to 64°C for the reference.
- **Mass Optimization and Performance Ranking:** The experimental data demonstrates that increasing the aluminum mass from 20 grams to 40 grams yields a progressive thermal benefit by minimizing localized thermal resistance. This firmly establishes Collector 3 as the 1st place configuration, followed by Collector 2 in 2nd place, and Collector 1 as the 3rd place reference system.

Future Recommendations

- Test higher mass increments of aluminum shavings (such as 60 grams and 80 grams) to discover the exact threshold where additional mass limits fluid flow or ceases to provide a thermal advantage.
- Investigate alternative recycled industrial waste materials, like copper or brass shavings, to evaluate their economic and thermal suitability compared to aluminum.
- Perform long-term durability testing on the adhesive binding layer to ensure the composite surface can withstand high stagnation temperatures without degrading.

References

[1] J. A. Duffie and W. A. Beckman, *Solar Engineering of Thermal Processes*, 4th ed. Hoboken, NJ, USA: Wiley, 2013.

[2] S. A. Kalogirou, *Solar Energy Engineering: Processes and Systems*. Burlington, MA, USA: Academic Press, 2009.

[3] International Renewable Energy Agency (IRENA), *Renewable Energy Statistics 2023*. Abu Dhabi, United Arab Emirates: IRENA, 2023.

[4] S. A. Kalogirou, “Solar thermal collectors and applications,” *Progress in Energy and Combustion Science*, vol. 30, no. 3, pp. 231–295, 2004.

[5] G. N. Tiwari and H. N. Singh, *Solar Distillation Systems*. New Delhi, India: Narosa Publishing House, 2008.

[6] A. E. Kabeel and M. M. Hamed, “Performance of flat plate solar collector systems,” *Renewable Energy*, 2005.

[7] K. Lovegrove and W. Stein, *Concentrating Solar Power Technology*. Cambridge, U.K.: Woodhead Publishing, 2012.

[8] International Renewable Energy Agency (IRENA), *Renewable Power Generation Costs in 2023*. Abu Dhabi, United Arab Emirates: IRENA, 2023.

[9] G. N. Tiwari and M. K. Ghosal, *Renewable Energy Resources*. New Delhi, India: Narosa Publishing House, 2007.

[10] D. Y. Goswami, F. Kreith, and J. F. Kreider, *Principles of Solar Engineering*. Philadelphia, PA, USA: Taylor & Francis, 2000.

[11] T. Mancini et al., “Concentrating solar power technology: Status and outlook,” *Energy Procedia*, 2014.

[12] M. M. El-Sebaii, “Flat-plate solar collector performance with coated and uncoated glass cover,” *Drying Technology*, 2006.

[13] R. Karlsson and B. Karlsson, “Thermal advantages for solar heating systems with a glass cover with antireflection surfaces,” *Solar Energy*, 2005.

[14] Z. Chen et al., “Advanced spectrally selective coatings for solar thermal applications,” *Renewable Energy*, 2020.

[15] A. Hernández-Guerrero et al., “Investigation of thermal behavior of water flow in solar collectors,” *Journal of Applied Research and Technology*, 2020.

[16] M. A. Habib et al., “Heat transfer enhancement in solar collector tubes using nanofluids,” *Engineering, Technology & Applied Science Research*, 2022.

[17] C. E. Kennedy, “Review of mid- to high-temperature solar selective absorber materials,” National Renewable Energy Laboratory (NREL), Technical Report, Golden, CO, USA, 2002.

[18] F. A. Al-Sulaiman et al., “Latest advances on solar thermal collectors: A review,” *Renewable and Sustainable Energy Reviews*, 2019.

[19] A. Ali et al., “Thermal performance investigations of flat plate solar collectors,” *Journal of Thermal Analysis and Calorimetry*, 2025.

[20] M. A. Kalogirou, “Recent advances in solar thermal collectors and systems,” *Renewable Energy*, 2020.

[21] H. Youcef et al., “Thermal performance analysis of solar collector components using numerical modeling,” *Applied Thermal Engineering*, 2022.

[22] T. V. Kadam, S. Y. Pakhare, and A. B. Godse, “Performance analysis of solar thermal collectors: A comprehensive review,” *Measurement: Energy*, 2025.

[23] M. L. Trejos Moncada et al., “Comparative experimental study of new absorbent surface coatings for flat plate solar collectors,” in *Proc. ISES Solar World Congress*, 2013.

[24] N. A. Pratik et al., “Experimental performance investigation of flat plate solar collector based on contact materials,” *Case Studies in Thermal Engineering*, 2023.

[25] T. Tiwari, “PVT systems: Review and applications,” *Renewable Energy*, 2015.

[26] B. Bansal et al., “Solar air heaters: A review,” *Renewable and Sustainable Energy Reviews*, 2010.

[27] H. Hollands, “Unglazed solar collectors performance,” *Solar Energy*, 2005.

[28] S. B. Riffat and X. Zhao, “ICS solar water heaters,” *Applied Energy*, 2007.

[29] A. Aste et al., “PV/T systems performance review,” *Energy and Buildings*, 2014.

[30] Duffie, J.A., Beckman, W.A,Solar Engineering of Thermal Processes, 5th Edition, Wiley, 2020.

[31] Incropera, F.P., DeWitt, D.P**,**Fundamentals of Heat and Mass Transfer, Wiley.

[32] ASHRAE Handbook – Fundamentals, 2021.